

Estimation of Building Height from ICESat-2/ATLAS and Airborne LiDAR Data Using Machine Learning Algorithms

Master of Science
in Geomatics Engineering

by
Aslıhan Yücel
ORCID 0000-0002-6917-942X

October, 2023

This is to certify that we have read the thesis **Estimation of Building Height from ICESat-2/ATLAS and Airborne LiDAR Data Using Machine Learning Algorithms** submitted by **Ashhan Yücel**, and it has been judged to be successful, in scope and in quality, at the defense exam and accepted by our jury as a MASTER'S THESIS.

APPROVED BY:

Advisor: **Assist. Prof. Dr. Müge Ağca**
İzmir Kâtip Çelebi University

Committee Members:

Assoc. Prof. Dr. Zeynel Abidin Polat
İzmir Kâtip Çelebi University

Assist. Prof. Dr. Fatih Adıgüzel
Bitlis Eren University

Date of Defense: October 19, 2023

Declaration of Authorship

I, **Aslıhan Yücel**, declare that this thesis titled **Estimation of Building Height from ICESat-2/ATLAS and Airborne LiDAR Data Using Machine Learning Algorithms** and the work presented in it are my own. I confirm that:

- This work was done wholly or mainly while in candidature for the Master's / Doctoral degree at this university.
- Where any part of this thesis has previously been submitted for a degree or any other qualification at this university or any other institution, this has been clearly stated.
- Where I have consulted the published work of others, this is always clearly attributed.
- Where I have quoted from the work of others, the source is always given. This thesis is entirely my own work, with the exception of such quotations.
- I have acknowledged all major sources of assistance.
- Where the thesis is based on work done by myself jointly with others, I have made clear exactly what was done by others and what I have contributed myself.

Date: 19.10.2023

Estimation of Building Height from ICESat-2/ATLAS and Airborne LiDAR Data Using Machine Learning Algorithms

Abstract

The height of buildings in cities are of critical importance to urban planning and sustainable growth, as these factors are closely linked to environmental, economic, social, and aesthetic elements that shape the structure and character of cities. The main purpose of this study is to calculate building heights using machine learning algorithms based on airborne LiDAR and ICESat-2 data in urban areas. Sub-objectives of the study to achieve the main objective are: (a) investigate the relationships between spaceborne and airborne LiDAR data and integrate the data, (b) investigate the performance of various machine learning algorithms that can be used in point cloud analysis when ICESat-2/ATLAS and airborne LiDAR data are analyzed, and (c) comparing the accuracy of building height data obtained from both spaceborne and airborne LiDAR systems with data obtained from ground-based measurement techniques. Airborne LiDAR data provided by GDM were used for the study. LiDAR points corresponding to the projection of each ICESat-2/ATLAS photon in the study area were selected. Python libraries were used to analyze the LiDAR data. Machine learning algorithms (K-Nearest Neighbors (K-NN), Random Forest (RF), Support Vector Machines (SVM), Artificial Neural Networks (ANNs) and RANSAC) were used to obtain highly accurate data by removing ground points. The results of the

classification processes indicate that the classification accuracy of the ICESat-2 data using the RF algorithm (strong beams RF = 96.83%, weak beams RF = 95.72%) is higher than that of the other algorithms used (strong beams K-NN = 94.08%, SVM = 75.43%, ANN = 77.60%, RANSAC = 71.68%, weak beams K-NN = 94.26%, SVM = 72.11%, ANN = 75.46%, RANSAC = 66.17%). In the classification of airborne LiDAR data, the classification accuracy of the K-NN and RF algorithms (K-NN = 99.99%, RF = 99.98%) was found to be higher than that of the other algorithms (SVM = 91.11%, ANN = 98.48%, RANSAC = 53.66%). After an initial analysis of the point clouds, digital elevation and terrain models were created for the study area. The resulting point clouds and elevation models were used to calculate building heights in the area. A regression model was created to examine the relationship between the systems used within the scope of the study, and statistical metrics were computed. After removing outlier values, the relationship between field measurement-airborne LiDAR ($R^2 = 0.9985$, RMSE = 0.1354, MSE = 0.0183, MAE = 0.0942, ME = 0.0388), field measurement-ICESat-2 ($R^2 = 0.9905$, RMSE = 0.3527, MSE = 0.1244, MAE = 0.2548, ME = -0.0610) and airborne LiDAR- ICESat-2 ($R^2 = 0.9921$, RMSE = 0.3209, MSE = 0.1029, MAE = 0.2314, ME = -0.0978) proved to be superior.

Keywords: ICESat-2/ATLAS, machine learning algorithm, building height, airborne LiDAR

Makine Öğrenmesi Algoritmaları Kullanılarak ICESat-2/ATLAS ve Havasal LiDAR Verilerinden Bina Yüksekliğinin Tahmini

ÖZ

Şehirlerdeki bina yükseklikleri, kent planlaması ve sürdürülebilir büyüme için hayati bir öneme sahiptir, çünkü bu faktörler şehirlerin yapısını ve karakterini belirleyen çevresel, ekonomik, sosyal ve estetik etmenlerle yakından ilişkilidir. Bu çalışmanın temel amacı, kentsel alanlarda havasal LiDAR ve ICESat-2 verilerine dayalı makine öğrenme algoritmalarını kullanarak bina yüksekliklerini hesaplamaktır. Ana hedefi gerçekleştirmek için çalışmanın alt amaçları şunlardır: (a) uzaysal ve havasal LiDAR verileri arasındaki ilişkileri araştırmak ve verileri birbirleri ile entegre etmek, (b) ICESat-2/ATLAS ve havasal LiDAR verileri analiz edildiğinde nokta bulutu analizinde kullanılacak çeşitli makine öğrenme algoritmalarının performansını incelemek ve (c) uzaysal ve havasal LiDAR sistemlerinden elde edilen bina yüksekliği verilerinin yersel ölçme tekniklerinden elde edilen verilerle doğruluğunu karşılaştırmak. Çalışma kapsamında HGM tarafından temin edilen havasal LiDAR verileri kullanılmıştır. Çalışma alanındaki her bir ICESat-2/ATLAS fotonunun izdüşümüne karşılık gelen havasal LiDAR noktalarının seçimi yapılmıştır. LiDAR verilerinin analizinde Python yazılım dili içerisindeki kütüphaneler kullanılmıştır. Zemin noktalarının çıkarılması için makine öğrenmesi algoritmaları (K-en yakın komşu (K-NN), destek vektör makineleri (DVM), rastgele orman (RO), yapay sinir

ağları (YSA) ve RANSAC) kullanılarak yüksek doğrulukta veriler elde edilmeye çalışılmıştır. Sınıflandırma işlemlerinin sonucunda ICESat-2 verilerinin sınıflandırılmasında RO algoritması ile sınıflandırma doğruluğunun (güçlü ışın RO = %96.83, zayıf ışın RO= %96.14) kullanılan diğer algoritmaların sınıflandırma doğruluğundan (güçlü ışın K-NN = %94.08, DVM = %75.43, YSA = %77.60, RANSAC = %71.68, zayıf ışın K-NN = %94.26, DVM = %72.11, YSA = %75.46, RANSAC = %66.17) daha iyi olduğu görülmüştür. Havasal LiDAR verilerinin sınıflandırılmasında K-NN ve RO algoritmaları ile sınıflandırma doğruluklarının (K-NN = %99.99, RO = %99.98) kullanılan diğer algoritmaların sınıflandırma doğruluğundan (DVM = %91.11, YSA = %98.48, RANSAC = %53.66) daha yüksek olduğu görülmüştür. Çalışmada nokta bulutu ön analiz işlemleri gerçekleştirildikten sonra çalışma alanına ait sayısal yükseklik ve sayısal arazi modelleri oluşturulmuş ve elde edilen nokta bulutları ve yükseklik modellerinden elde edilen veriler kullanılarak alandaki bina yükseklikleri hesaplanmıştır. Çalışma kapsamında kullanılan sistemler arasındaki ilişkiyi incelemek için regresyon modeli oluşturulmuş ve istatistiksel metrikler hesaplanmıştır. Aykırı değerler çıkarıldıktan sonra arazi ölçümleri-havasal LiDAR arasındaki ilişkinin ($R^2 = 0.9985$, RMSE = 0.1354, MSE = 0.0183, MAE = 0.0942, ME = 0.0388), arazi ölçümleri-ICESat-2 arasındaki ($R^2 = 0.9905$, RMSE = 0.3527, MSE = 0.1244, MAE = 0.2548, ME = -0.0610) ve havasal LiDAR-ICESat-2 arasındaki ilişkidir ($R^2 = 0.9921$, RMSE = 0.3209, MSE = 0.1029, MAE = 0.2314, ME = -0.0978) daha iyi olduğu görülmüştür.

Anahtar Kelimeler: ICESat-2/ATLAS, makine öğrenme algoritması, bina yüksekliği, havasal LiDAR

This thesis is dedicated to my beloved niece, Umay Ece Ünal, who passed away at a young age.

Acknowledgment

I would like to thank my esteemed supervisor, Assist. Prof. Dr. Mge Ađca, who supported and guided me throughout my studies and shared her knowledge and experience with me. I am also grateful to my valuable lecturers, Dr. Efdal Kaya, Prof. Dr. Mevlt Yetkin, and Prof. Dr. Femin Yalđın Kkbayrak, for their support during the period of my thesis. In addition, I would like to thank my colleague, Research Assistant Mert Kayalık, who supported me beyond measure during my fieldwork, and my colleague, Master Geomatic Engineer Ali İhsan Dalođlu, who was always there for me during the work on my thesis, answering all my questions and supporting me tirelessly. I would like to express my deepest gratitude to my parents, especially my mother, as well as my father and siblings, who always stood behind me and supported me tirelessly. I am also grateful to my dear niece and nephews, Umay Ece, Alp Tuđra and Bertuđ Arslan, who brought joy into my life during difficult times.

Table of Contents

Declaration of Authorship	ii
Abstract	iii
Öz	v
Acknowledgment	viii
List of Figures	xi
List of Tables.....	xiii
List of Abbreviations.....	xiii
1 Introduction	1
2 Systems	5
2.1 Airborne LiDAR System	5
2.2 Spaceborne LiDAR System (ICESat-2/ATLAS).....	6
2.3 Satellite-based and Terrestrial Measurement Systems	10
2.3.1 Total Station	10
2.3.2 Global Positioning System (GPS)	10
2.4 Machine Learning Algorithms	10
2.4.1 Random Forest (RF)	11
2.4.2 Random Sample Consensus (RANSAC).....	12
2.4.3 Artificial Neural Networks (ANNs)	12
2.4.4 Support Vector Machine (SVM)	13
2.4.5 K-Nearest Neighbor(K-NN).....	14
3 Implementation.....	15
3.1 Study Area	15

3.2	Material and Method.....	16
3.2.1	Processing of Airborne LiDAR Data.....	16
3.2.2	Processing of ICESat-2/ATLAS Data	19
3.2.3	Field Measurement Data.....	21
3.2.4	Classification Processing with Machine Learning Algorithms	23
3.2.5	Accuracy Analysis of Algorithms	24
4	Results and Discussions.....	26
4.1	Field Measurement-Airborne LiDAR Accuracy Assessment.....	30
4.2	Field Measurement-ICESat-2/ATLAS Accuracy Assessment	32
4.3	Airborne LiDAR-ICESat-2/ATLAS Accuracy Assessment.....	33
5	Conclusion.....	35
	References	37
	Appendix.....	46
	Appendix Publications from the Thesis.....	47
	Curriculum Vitae	48

List of Figures

Figure 2.1	General concept of airborne LiDAR system	6
Figure 2.2	ICESat/GLAS system, which performs measurements in Earth's orbit ...	7
Figure 2.3	ICESat-2/ATLAS system and the areas where it obtains data.....	8
Figure 2.4	Sampling geometry of ICESat-2/ATLAS	8
Figure 2.5	ICESat-2/ATLAS data products.....	9
Figure 2.6	Random Forest algorithm scheme.....	11
Figure 2.7	A operating logic of ANN.....	13
Figure 2.8	Logic of the SVM algorithm	14
Figure 2.9	Logic of the K-NN algorithm.....	14
Figure 3.1	Study area.....	15
Figure 3.2	Airborne LiDAR data with noise points	17
Figure 3.3	Airborne LiDAR data without noise points	17
Figure 3.4	Classified airborne LiDAR data a) Ground, b) Non-ground.....	17
Figure 3.5	Digital models obtained from airborne LiDAR data a) Digital Terrain Model, b) Digital Surface Model	18
Figure 3.6	Overlaid ICESat-2/ATLAS and DSM.....	20
Figure 3.7	Specifications of the TOPCON GR-5	22
Figure 3.8	Specifications of the TOPCON OS-101.....	22
Figure 3.9	Confusion matrix.....	24
Figure 4.1	The heights obtained for the 70 buildings.....	28
Figure 4.2	Photos of building number 65, (a) From 2016, (b) From 2022.....	29
Figure 4.3	Photos of building number 70, (a) From 2016, (b) From 2022.....	30
Figure 4.4	Photos of building number 90, (a) From 2016, (b) From 2022.....	30
Figure 4.5	Field Measurement-Airborne LiDAR linear regression, (a) With height data of 70 buildings, (b) With height data of 67 buildings	31

Figure 4.6 Field Measurement-ICESat-2/ATLAS linear regression, (a) With height data of 70 buildings, (b) With height data of 67 buildings 32

Figure 4.7 Airborne LiDAR-ICESat-2/ATLAS linear regression, (a) With height data of 70 buildings, (b) With height data of 67 buildings 33

List of Tables

Table 3.1	Optech Pegasus HA-500 technical specifications	16
Table 3.2	ICESat-2/ATLAS data and shift amounts on axes.....	20
Table 4.1	Accuracy analysis of the classification results of ICESat-2/ATLAS.....	26
Table 4.2	Accuracy analysis of the classification results of airborne LiDAR	26

List of Abbreviations

ANNs	Artificial Neural Networks
ATLAS	Advanced Topographic Laser Altimeter System
CORS	Continuously Operating Reference System
DHM	Digital Height Model
DSM	Digital Surface Model
DTM	Digital Terrain Model
EDM	Electronic Distance Measurement
GDM	General Directorate of Mapping
GPS	Global Positioning System
ICESat-2	Ice, Cloud and Land Elevation Satellite-2
IMU	Inertial Measurement Unit
K-NN	K-Nearest Neighbors
LiDAR	Light Detection and Ranging
NASA	National Aeronautics and Space Administration
OBIA	Object-Based Image Analysis
PALS	Portable Airborne Laser System
RANSAC	Random Sample Consensus
RF	Random Forest
RTK	Real Time Kinematic
SOR	Statistical Outlier Filter
SVM	Support Vector Machines
TG20	Turkey Geoid 2020

TIN	Triangulated Irregular Network
VHR	Very High Resolution

Chapter 1

Introduction

In urban areas, the determination of building heights is of crucial importance for urban planning and development. This issue plays a critical role in the transformation and sustainable growth of cities. Building heights are intertwined with environmental, economic, social, and aesthetic factors, and these interactions shape the structure and character of a city. Accurately determining building heights in urban areas is a balancing act that must take into account a variety of factors, such as population growth, infrastructure requirements, transportation efficiency, green spaces, and public access. Building heights are a fundamental factor for 3D urban models. Building heights can be used to obtain many necessary parameters. The building height parameter helps to more accurately predict data such as population distribution [18], greenhouse gas emissions [19], energy consumption estimation [20] urban albedo [21], material stock allocation [22], human well-being and urban heat island effects [23].

Airborne LiDAR is an advanced laser scanning system that uses sophisticated technology to capture precise and detailed three-dimensional data of the Earth's surface. Due to its high sensitivity and accuracy, it is used in a wide range of applications [24]. Studies have shown that airborne LiDAR has achieved successful results in several areas such as land cover classification, forest stand height mapping, seafloor bathymetric mapping, seafloor change detection, archaeological feature and landform identification, and obtaining 3-dimensional building morphology parameters [25,26,27,28,29].

Zhang et al. [7] developed an improved morphological filter for detecting non-ground points (vehicles, vegetation, and buildings) from airborne LiDAR data. González-González-Aguilera et al. [30] applied a Triangulated Irregular Network (TIN) model

to airborne LiDAR point cloud data. Using this model, buildings were automatically detected and data such as height, area, and volume were obtained for each building. Wang and Li [32] used Very High Resolution (VHR) satellite images and airborne LiDAR data acquired after the 2010 Haiti earthquake to compare with pre-earthquake VHR satellite images and were able to detect damage to urban buildings by comparing building heights. Zhang et al. [33] created digital models (DHM, DSM, DTM) from airborne LiDAR data. Color-infrared aerial photos was used to detect trees from the DHM. The object-based image analysis method (OBIA) was used to identify buildings and calculate their height. Zhou and Neumann [31] applied the Support Vector Machine (SVM) algorithm to the airborne LiDAR data in their study and developed an automatic building modeling algorithm by separating roof and ground points from tree points. In the study conducted by Zhou and Gong [34], a deep neural network approach was proposed for building detection and extraction from airborne LiDAR data. Shirowzhan et al. [35] used temporal lidar data to determine building height values. Various algorithms were used in processing these data, including machine learning and point-based methods. As a result, the effectiveness of existing algorithms was investigated.

The ICESat-2 satellite was launched into Earth orbit on September 15, 2018, and is equipped with a laser altimeter called ATLAS (Advanced Topographic Laser Altimeter System), which uses single photon counting sensitivity. ATLAS uses green (532 nm) laser light to measure surface elevation [36]. ICESat-2 data have been utilized for studies in several areas, including sea ice thickness [37], sea ice wave analysis [38], ice sheet surface height [39], inland water height [40], ground height [41], and vegetation height [9].

Smith et al. [42] developed an algorithm to estimate ice sheet surface height from the ICESat-2/ATLAS dataset. They also evaluated the performance of this algorithm on land-ice surfaces and under various cloud conditions. In their study, Ma et al. [43] tested the usability of ICESat-2/ATLAS and Sentinel-2 image datasets to create bathymetric maps. In their study, Agca and Daloglu [44] used the TG20 dataset and local GPS leveling points to determine the geoid and orthometric heights of ground points received from ICESat-2/ATLAS, airborne LiDAR and GNSS/CORS systems. In their study, Wang et al. [41] compared the effectiveness of ICESat-2 dataset with

airborne LiDAR data for predicting surface elevation on the Earth's surface. In their study, Zhang et al. [45] compared performance of the ICESat-2 dataset, specifically ATL06, in predicting the elevation of glaciers in the Qilian Mountains with data obtained from CORS (Continuously Operating Reference Stations) and UAV (Unmanned Aerial Vehicle) measurements. In their study, Zhang et al. [46] compared the performance in obtaining Leaf Area Index (LAI) from ICESat-2/ATLAS data with that obtained from MODIS and Sentinel-2 data. Neuenschwander et al. [9] in their study compared the performance of terrain and canopy height estimation in the boreal forest region of southern Finland using ICESat-2/ATLAS data with results obtained from airborne LiDAR data. Tiwari and Narine [47] compared machine learning algorithms and geostatistical approaches to estimate forest canopy height in the southeastern United States using data from the ICESat-2/ATLAS system. In their study, Narine et al. [48] utilized height data from the ICESat-2/ATLAS system and multispectral data from Landsat to estimate forest biomass using deep learning algorithms. In their study, Lian et al. [49] proposed a method that used data from the ICESat-2/ATLAS system to extract high accuracy ground control points in urban areas. Due to the novelty of the ICESat-2/ATLAS data, there are relatively few studies in the literature that have used it for building height analysis. Preliminary searches have revealed that there are few studies that specifically address the calculation of building heights using ICESat-2/ATLAS data. In their study, Dandapanthula et al. [50] used photon data from the ICESat-2/ATLAS system to estimate the height of buildings and compared these estimates with field measurements. Wu [11] proposed a method in her master's thesis using data from the ICESat-2/ATLAS system to estimate the height of all buildings in the Netherlands. In the study conducted by Zhao et al. [51], airborne LiDAR and ICESat-2 data were utilized to extract surface heights in urban areas. DTM and DSM raster models were created using airborne LiDAR data. These raster models were then matched with ICESat-2/ATLAS data to calculate building heights. In the study conducted by Lao et al. [52], building heights in urban areas were calculated using data from ICESat-2/ATLAS and terrestrial LiDAR systems.

The scope of this study is the calculation of building heights in urban areas. In this study, ICESat-2/ ATLAS, airborne LiDAR data and machine learning algorithms were used to calculate heights. The sub-objectives of the study to achieve the main objective are: (a) investigate the relationships between spaceborne and airborne LiDAR data and

integrate the data, (b) investigate the performance of various supervised and unsupervised machine learning algorithms that can be used in point cloud analysis when ICESat-2/ATLAS and airborne LiDAR data are analyzed, and (c) comparing the accuracy of building height data obtained from both spaceborne and airborne LiDAR systems with data obtained from field measurement.

Chapter 2

Systems

2.1 Airborne LiDAR System

LiDAR is now a widely used technology for various purposes. These systems are very popular for quickly obtaining high-precision, reference-based 3D data. LiDAR measures the time it takes for a laser pulse to travel from an aerial vehicle to a target on the surface and reflect back to the sensor [4]. LiDAR systems are classified into three main groups according to the platforms they are mounted on. These groups are airborne, terrestrial, and spaceborne. Airborne LiDAR systems typically measure the X, Y and Z coordinates of reflective objects scanned by LiDAR sensors beneath aerial vehicles. As a result of these measurements, three-dimensional point clouds are obtained [7]. An airborne LiDAR system consists of a LiDAR sensor that generates laser beams and measures time it takes for these beams to reach the ground and return after they are reflected from the ground, GPS, to track the position of the aircraft, IMU, to monitor the accelerations and orientation of the aircraft in the air, and on-board systems to store the data of the scanned area. The system is deployed on an aircraft (airplane or helicopter) [2]. The general concept of airborne LiDAR system is shown in figure 2.1. Another type of airborne LiDAR is PALS (Portable Airborne Laser System). PALS the LiDAR developed in 1999 by NASA (National Aeronautics and Space Administration) employee Dr. Ross Nelson differs from other LiDAR systems but is similar to an airborne LiDAR system in terms of the data collection method [1].

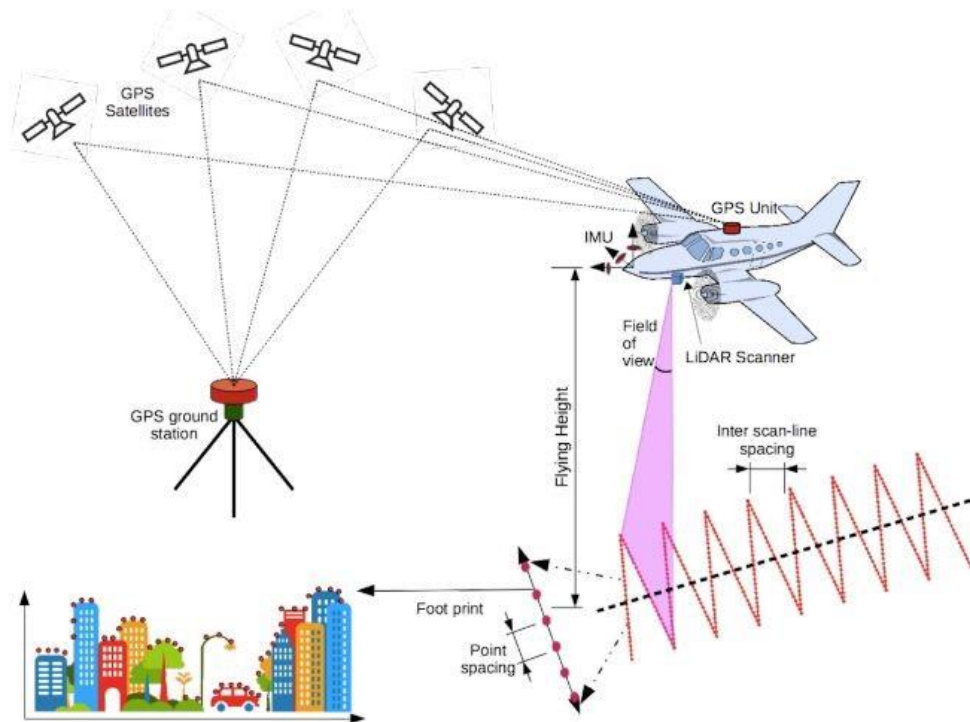


Figure 2.1: General concept of airborne LiDAR system [2].

2.2 Spaceborne LiDAR System (ICESat-2/ATLAS)

The ICESat/GLAS system is widely recognized as the world's first space-based laser scanning system [5]. Launched in 2003, the ICESat satellite contains the GLAS laser sensor, forming an integrated system. The main objective of this system is to monitor changes in polar ice and collect topographic data of the Earth's surface [3]. The ICESat/GLAS system generates laser beams with wavelengths of 1064 nm and 532 nm. The frequency value for the repetition rate of laser pulses is 40 Hz. The GLAS footprints directed at the Earth's surface have a nominal diameter of 70 meters and a spacing of 172 meters between successive footprints [1,6].

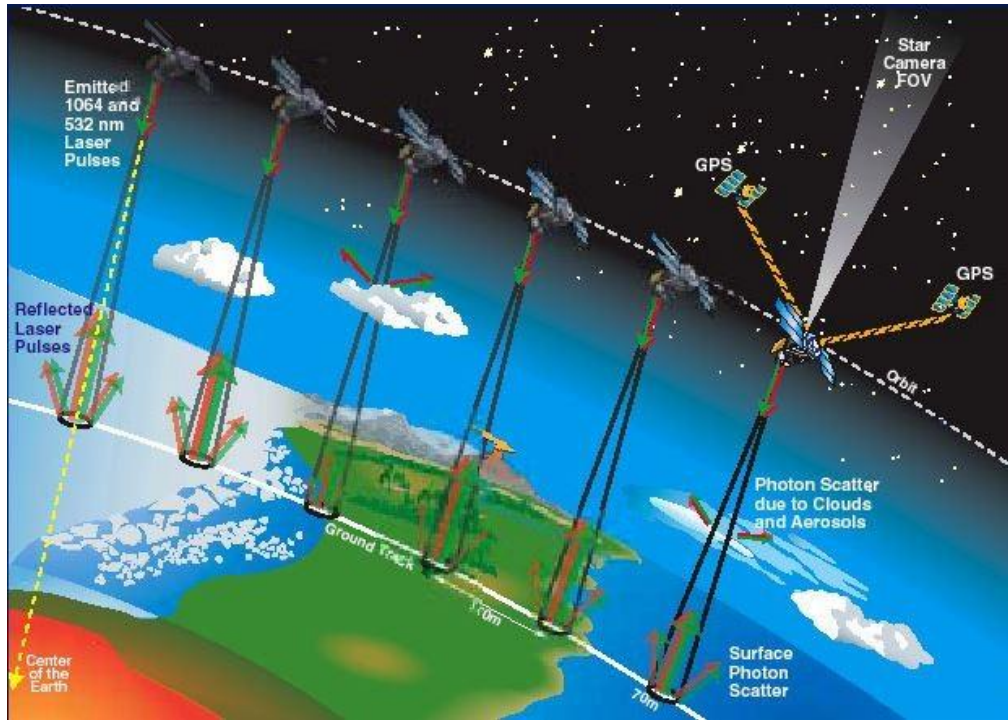


Figure 2.2: ICESat/GLAS system, which performs measurements in Earth's orbit [8].

The ICESat/GLAS mission, which successfully completed its mission between 2003 and 2009, has handed over its tasks to the ICESat-2/ATLAS system. This system was launched into orbit from NASA in 2018. ICESat-2 carries the ATLAS instrument, which uses photon-counting technology. ICESat-2/ATLAS LiDAR system provides data on glacier heights, sea ice heights, cloud layers, and more [9,10]. The orbital motion of ICESat-2 is shown in Figure 2.3. The ATLAS system transmits laser pulses at a repetition rate of 10 kHz to the Earth's surface. These laser pulses have a wavelength of 532 nm. The ATLAS sensor sends three pairs of beams to the Earth's surface, with each pair spaced 3.3 km apart. Each pair consists of a weak and a strong beam, spaced 90 m apart. The footprints created by the laser beams have a diameter of 17 m. [11,12]. The ICESat-2/ATLAS sampling geometry is shown in Figure 2.4. The data sets obtained from the ICESat-2/ATLAS system are shown in Figure 2.5.

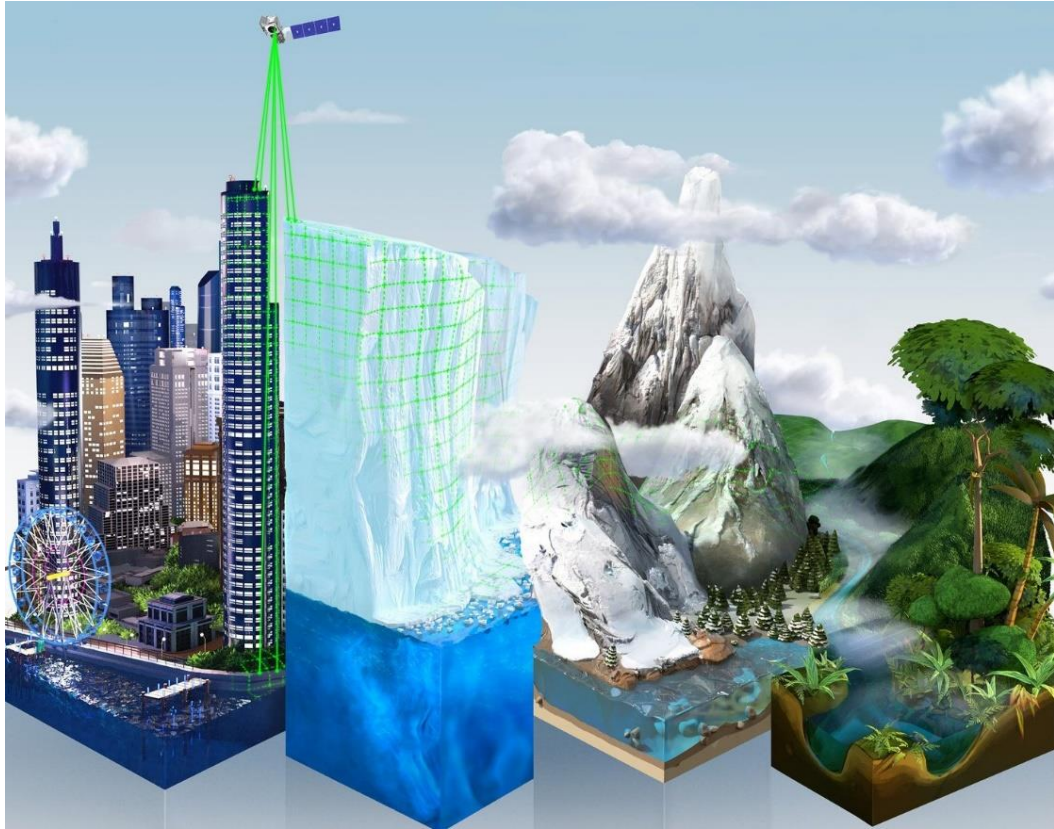


Figure 2.3: ICESat-2/ATLAS system and the areas where it obtains data [55].

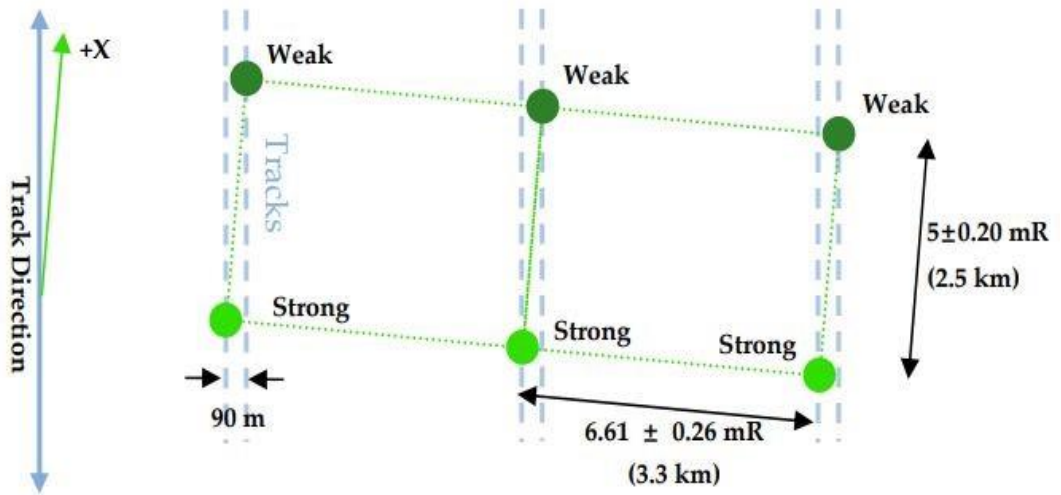


Figure 2.4: Sampling geometry of ICESat-2/ATLAS [13].

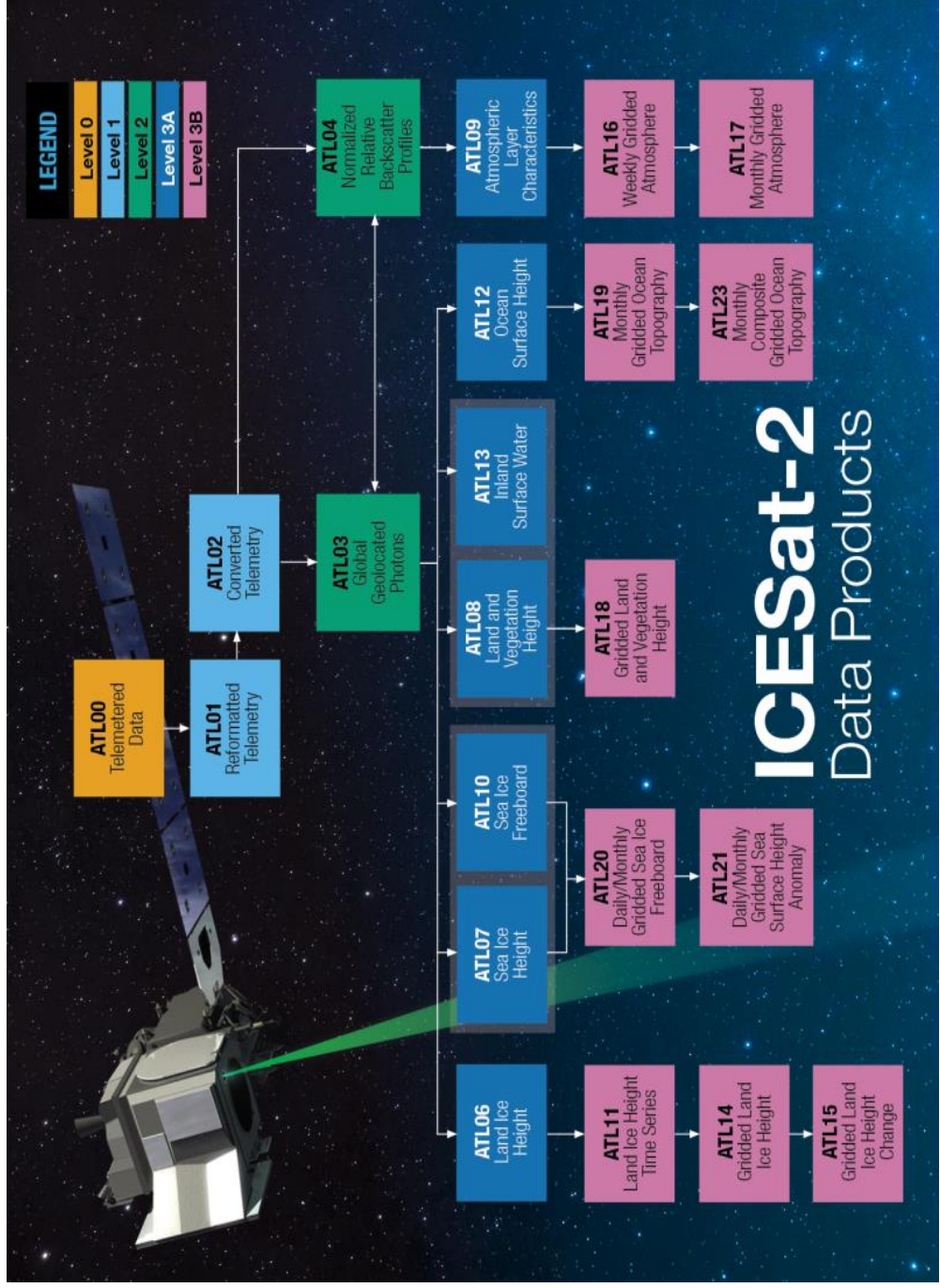


Figure 2.5: ICESat-2/ATLAS data products [14].

2.3 Satellite-based and Terrestrial Measurement Systems

2.3.1 Total Station

The total station is a measuring device used in terrestrial surveying. This device is used to measure horizontal and vertical angles and to determine distances. The total station determines the angles and distances of the measured point and allows to record its coordinate information (X, Y and Z). Total stations are made by taking inspiration from the working principle of two different electronic devices. Firstly, a system similar to electronic theodolites was used for horizontal and vertical angle measurements. Secondly, the system of electronic distance meters has been used for distance measurements [17].

2.3.2 Global Positioning System (GPS)

The satellite-based system GPS provides the necessary parameters for determining the positions of the Earth's points such as latitude, longitude and altitude. The system is based on the "resection method", an observation technique that can be used to determine the position from an unknown point to known points [15]. The GPS system consists of 24 satellites configured so that at least 6 satellites are continuously visible from any point on Earth, except the polar regions [16]. The GPS system was initially used in conjunction with classical Real-Time Kinematic (RTK) method. However, due to certain limitations of the classical RTK method, the CORS (Continuously Operating Reference Station) system was developed [53].

2.4 Machine Learning Algorithms

Computational processes that achieve specific results with input data without being preprogrammed are called machine learning algorithms. These algorithms perform iterative operations and modify their own structures, thereby learning to perform the given task more effectively. Machine learning algorithms are trained from datasets

comprising input data and corresponding target values. During the training process, the algorithm learns from the data and adjusts its internal parameters to optimize its performance. This enables the algorithm to make accurate predictions when faced with new and unseen data. By generalizing patterns from the training data, the algorithm should develop the ability to make meaningful inferences and predictions for new data instances it has not yet encountered. The learning process, on the other hand, is an ongoing process. Machine learning algorithms can be categorized into various types, including supervised and unsupervised learning. In supervised learning, the algorithm undergoes training using labeled data, which consists of input-output pairs. Contrary to supervised learning, unsupervised learning operates on unlabeled data, aiming to uncover patterns or structures within the data [54].

2.4.1 Random Forest (RF)

This algorithm created by combining the 'bootstrap aggregating' and 'random subspace method' techniques, performs classification using a collection of decision trees or decision tree ensembles. In the Random Forest algorithm, each decision tree is trained independently on the same dataset. Classification results are determined based on the most frequently occurring output value of the decision trees [59]. Random Forest is not only an effective method for classification problems with multiple classes, but also reduces the tendency of overfitting and improves the ability of generalization. The random forest algorithm scheme is shown in Figure 2.6.

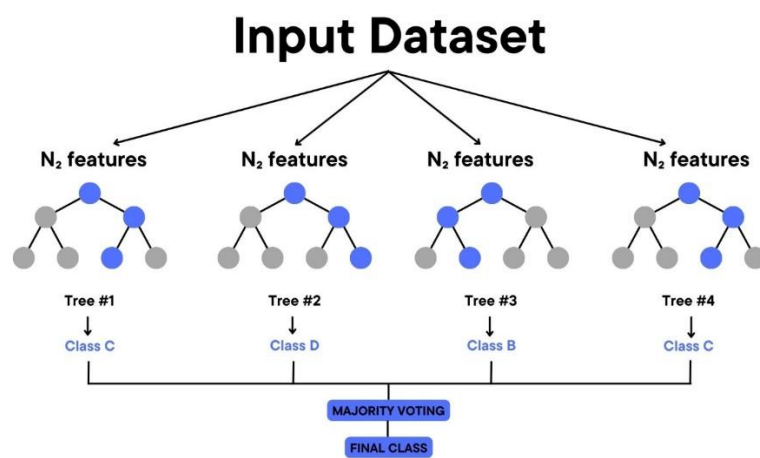


Figure 2.6: Random Forest algorithm scheme.

2.4.2 Random Sample Consensus (RANSAC)

The RANSAC algorithm, developed in 1981 by Fischler and Bolles [62], was designed for estimating model parameters and is capable of smoothing data with significant outliers. The algorithm is primarily used for plane estimation from three-dimensional point cloud data. The principle of operation of the algorithm is as follows:

Firstly, three random points are selected, and the plane parameters are calculated based on these points. Then, the algorithm determines which plane each of the other points in the point cloud belongs to based on a specified threshold. In this way, the points that best fit the plane can be determined. The threshold is a tolerance limit used to determine whether a point belongs to the plane. These steps are repeated N times. In each iteration, the number of points belonging to a particular plane is counted, and the quality of the plane is calculated using an error criterion. If the obtained result is better than the previous one, i.e. with fewer errors, the new plane parameters replace the old ones.

In a method based on RANSAC, no random starting point for the parameters is determined, but several parameter sets are created by selecting random points. Iterations are performed with this parameter set to obtain the best result. In the further iterations, the parameters with the best result are selected, which leads to the desired accuracy of the result.

2.4.3 Artificial Neural Networks (ANNs)

ANNs, is a model that simulates the functioning of the human brain and the decision-making process. Similar to biological neural networks, an artificial neural network is formed by connecting nodes. ANN is trained using two main categories of learning processes. These learning processes are supervised learning and unsupervised learning. The first type of learning, called supervised learning, uses a training set consisting of input data provided to the algorithm and matching output data for that input. Unsupervised learning, on the other hand, focuses solely on the recognition of input data [60]. An artificial neural network (ANN) usually consists of three layers.

Nodes in input are connected to nodes in hidden, and each node in hidden is connected to nodes in output. These connections enable the flow of information throughout the network. Raw data is fed into input layer and forwarded to hidden layer for processing. In the hidden layer, calculations and transformations are performed on the received information to extract relevant features. The values obtained in hidden section are then forwarded to output section. The output section combines the information from the input and hidden layers, performs the necessary operations, and generates the output data [61]. An example of the operating logic of ANN is shown in Figure 2.7.

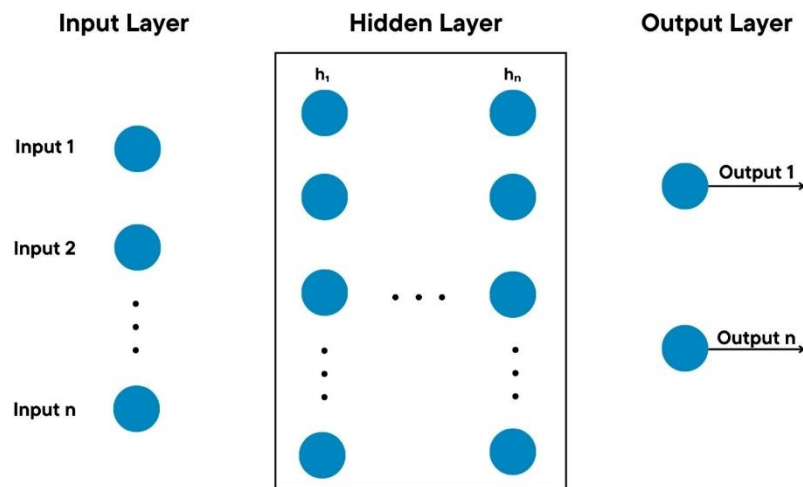


Figure 2.7: A operating logic of ANN.

2.4.4 Support Vector Machine (SVM)

SVM, is widely used and considered as one of the most advanced algorithms. SVM is used for regression and classification analysis. SVM algorithms can perform both linear and non-linear classifications. In non-linear classification, they draw margins using the "kernel trick" Margins are drawn to maximize the distance between classes and minimize classification errors (Figure 2.8). By transforming data from low-dimensional datasets into high-dimensional feature spaces, SVMs can make non-linear relationships more modelable. SVMs can provide effective results even with a low number of samples [57,58].

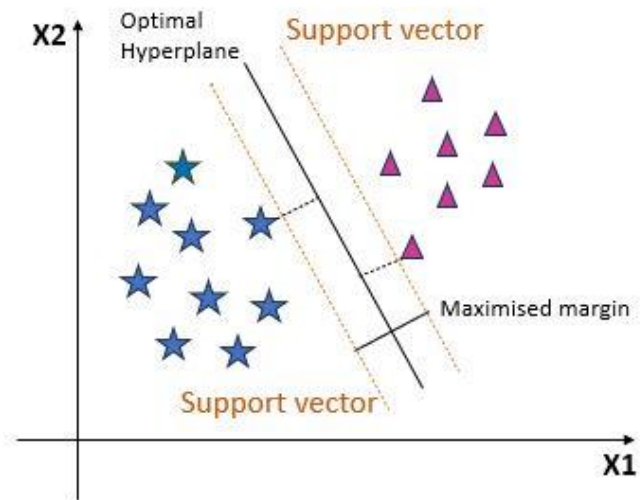


Figure 2.8: Logic of the SVM algorithm.

2.4.5 K-NN (K-Nearest Neighbor)

The K-NN algorithm is a straightforward machine learning algorithm that belongs to the supervised learning category. The K-NN algorithm is commonly employed for classification problems, although it can be utilized for both regression and classification tasks. The K-NN algorithm classifies a data point in the target dataset based on its proximity to previous data points [56]. By using feature similarity, K-NN predicts the values of new data points (Figure 2.9).

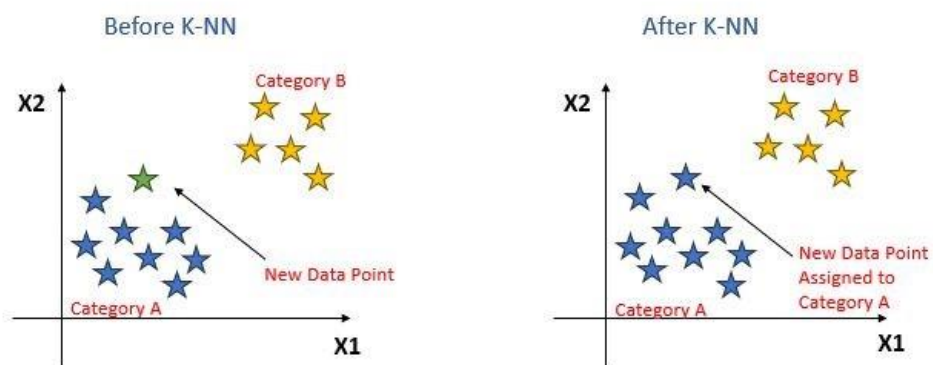


Figure 2.9: Logic of the K-NN algorithm.

Chapter 3

Implementation

3.1 Study Area

The district of Bergama, which is located in the northwest of the province of Izmir, was chosen as the study area for this thesis (Figure 3.1). The study area is located at an altitude of 68 meters above sea level and lies between $39^{\circ}06'13.02''$ - $39^{\circ}5'45.38''$ north latitude and $27^{\circ}9'58.11''$ - $27^{\circ}9'55.40''$ east longitude. The area was selected as the study area because the General Directorate of Mapping (GDM) provided airborne LiDAR test flight data for Bergama district. The study area encompasses various details including buildings, roads, water bodies, forests, and agricultural areas.

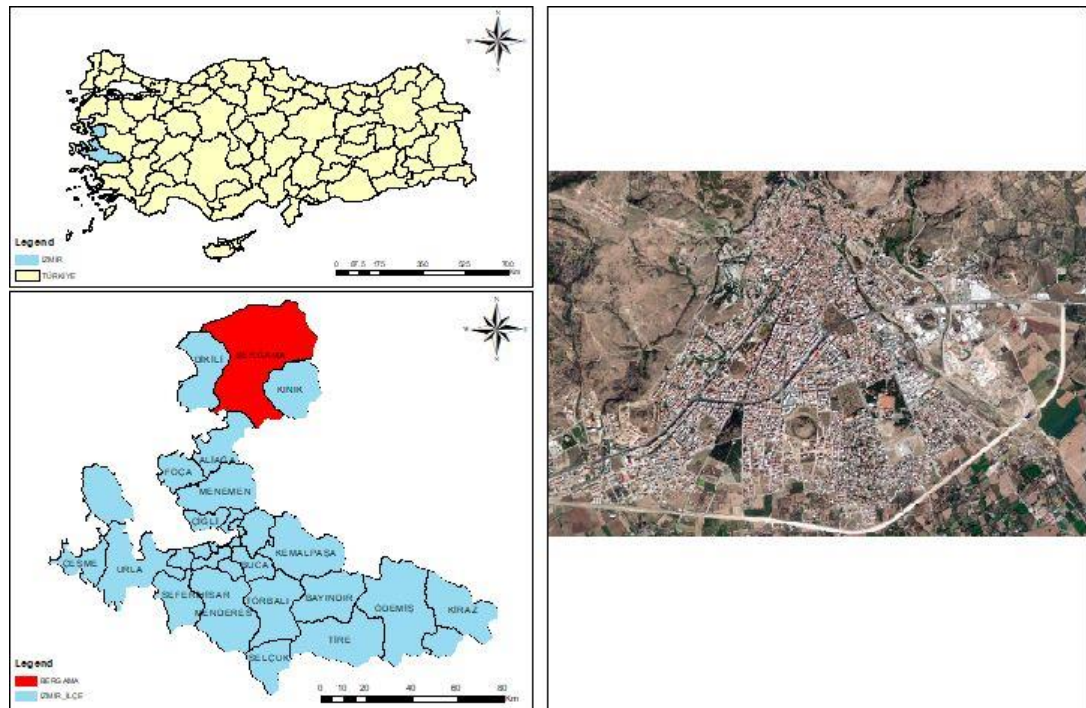


Figure 3.1: Study area.

3.2 Material and Method

3.2.1 Processing of Airborne LiDAR Data

Test flight data collected by the GDM were used for this study. In 2014, Optech Pegasus HA-500 system from Optech company was used to collect airborne LiDAR data from an altitude of 1200 m, 25% overlap, 32 columns, a scanning angle of 35°, and a scanning width of 580 m. Related to the Pegasus HA-500 system detailed information is shown in Table 3.1. The test area was selected based on the details it contains such as forests, buildings, and water, with Bergama district as the center. The test area covers about 156 km². Instead of using the entire test data, data from a 28 km² area with a high density of buildings was used, which is in line with the purpose of the study.

Table 3.1: Optech Pegasus HA-500 technical specifications

Flight Altitude	150-5000 m
Effective Laser Repetition Rate	100-500 kHz
Scanning Angle	0-75° Adjustable
Accuracy (MSE)	≤ 5-20 cm
Scanning Mechanism	Oscillating

In examining the airborne LiDAR data used in the study, it was specified that the data received from the GDM was unprocessed raw data. The raw data contains a significant amount of noise points that come from sunlight and various environmental factors (Figure 3.2). Therefore, it is necessary to clean the data from the noise points and classify the data before using it in the study. 32 airborne LiDAR data covering the study area were merged and noise points were removed from the merged data by applying a SOR filter (Figure 3.3). The filtered data that completed the filtering process was saved in a point cloud format with the extension (.las/laz). CloudCompare v2.11 software was used for these procedures.

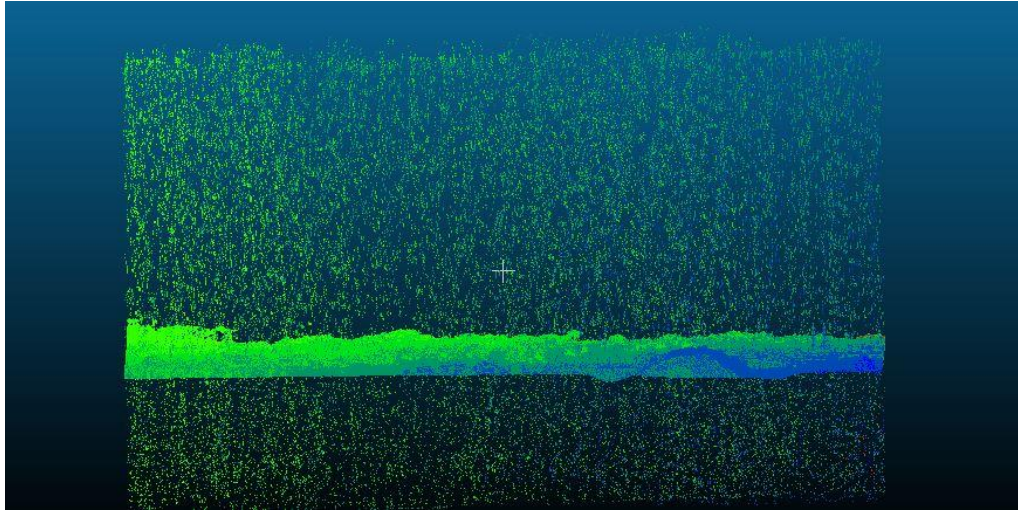


Figure 3.2: Airborne LiDAR data with noise points.

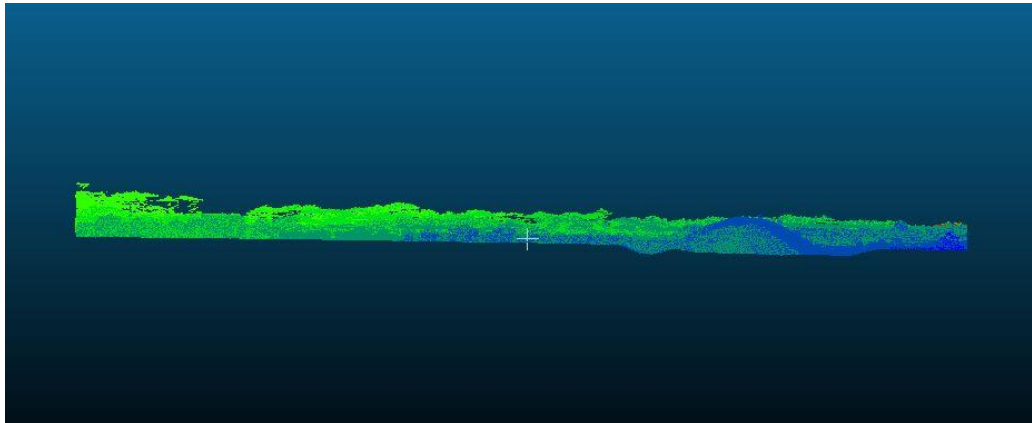
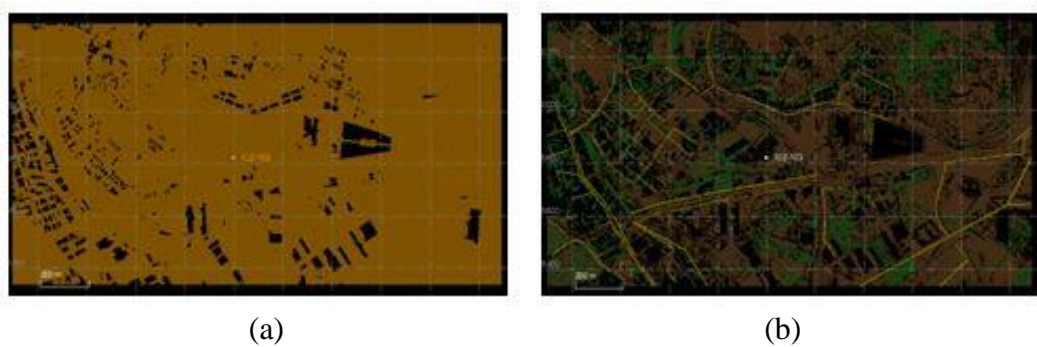


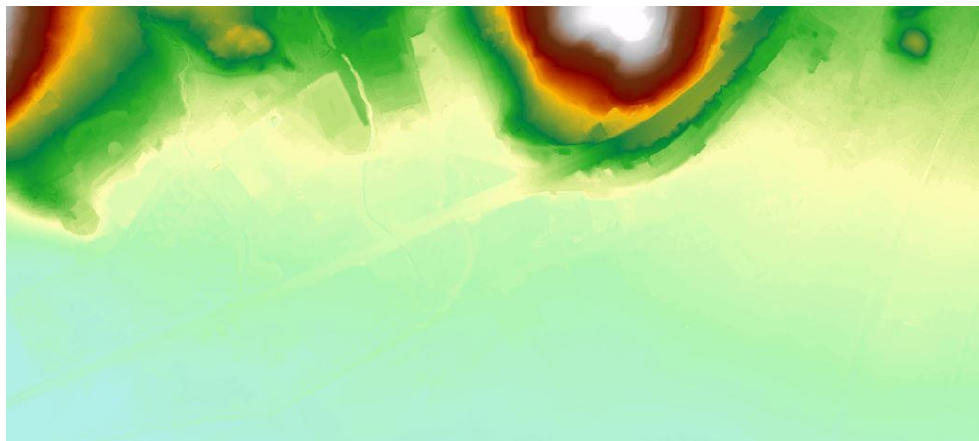
Figure 3.3: Airborne LiDAR data without noise points.

The unclassified point cloud data, cleaned from noise points, was classified utilizing Trimble Business Center v5.20 program. Two classes were formed during the classification process: ground and non-ground (Figure 3.4). The generated classified data was saved in point cloud format (.las/laz).

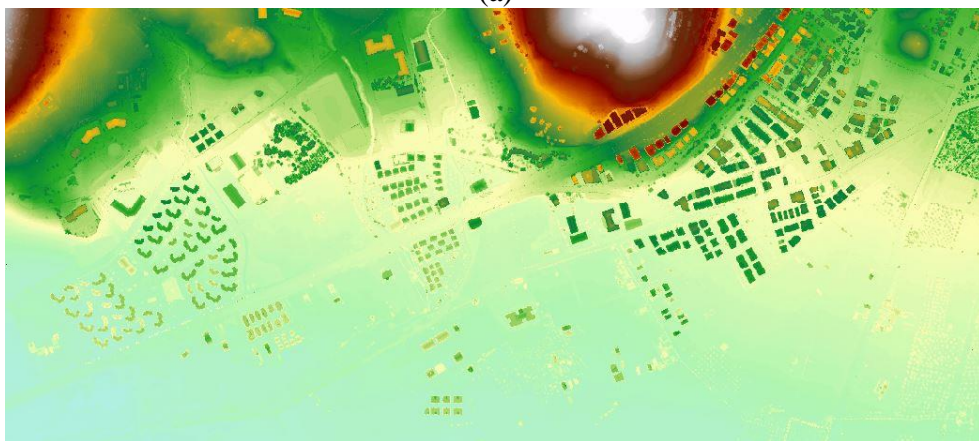


(a) (b)
Figure 3.4: Classified airborne LiDAR data a) Ground, b) Non-ground.

The coordinate system of the point cloud data acquired from airborne LiDAR data is defined as World Geodetic System (WGS84) Universal Transverse Mercator (UTM) 6° Zone 35. This airborne LiDAR data is used as a reference for the acquisition and alignment of ICESat-2/ATLAS data. To be used as a reference for ICESat-2/ATLAS data, digital models in raster data format are generated from the airborne LiDAR data. These generated raster data are called Digital Terrain Models (DTM) and Digital Surface Models (DSM). The resulting raster models (.tiff) were recorded with the extension. Airborne LiDAR data classified as ground was used to create a DTM, while airborne LiDAR data classified as ground and non-ground was used to create a DSM. ArcGIS v10.4 software was used to define the coordinate system of the classified point clouds and create the digital models. The digital models obtained from the LiDAR (Figure 3.5).



(a)



(b)

Figure 3.5: Digital models obtained from airborne LiDAR data a) DTM, b) DSM.

3.2.2 Processing of ICESat-2/ATLAS Data

All ICESat-2/ATLAS data within the study area were reviewed and the Track IDs for the data to be used in the study were determined. Data with track IDs 777, 1196, and 1219 provided by the ICESat-2/ATLAS system since the beginning of data provision were reviewed. In this study, for estimation of building heights from ICESat-2/ATLAS data, Global Geolocated Photon Data (ATL03) and Land Water Vegetation Elevation (ATL08) data were downloaded from the OpenAltimetry website. The downloaded data files have an (.h5) file extension. The ATL03 dataset product includes the latitude, longitude, elevation, and time information of each photon obtained from the ICESat-2/ATLAS system [63]. The ATL08 dataset product has been developed to determine terrain and vegetation heights based on the distribution of signal photons. The ATL08 product estimates the elevations of the ground surface and top of canopy by analyzing the distribution of individual photons. Subsequently, the individual photons are labeled as noise, ground, canopy, or top of canopy photons [64]. Integration of the ATL03 and ATL08 datasets is important to associate position and surface information with X, Y, and Z data for the study area. This integration allows consolidation of both local position information and surface features into a single dataset. In this way, more comprehensive and meaningful results can be obtained [44]. The process of associating ATL03 and ATL08 data was performed using PhoREAL v3.30 and Python v3.9 software. For the association process, the ATL03 and ATL08 data were first loaded into the software. In the previous step, a DTM generated from airborne LiDAR data and saved in (.tiff) format was selected as reference data. The amounts of displacement in the ICESat-2/ATLAS data were detected, and a shifting process was performed on the data in the X and Y axes. The amounts of displacement in the ICESat-2/ATLAS data are presented in Table 3.2. The time (Time (sec), Delta Time (sec)), location information (Latitude (deg), Longitude (deg), UTM Easting (m), UTM Northing (m)), elevation information (Ellipsoidal (m HAE), Orthometric (MSL)), classification, and signal confidence values were obtained from the photon data acquired from the ICESat-2/ATLAS system. The signal confidence values of the photons (0-noise, 1-background, 2-low, 3-medium, 4-high) and classification values (0-noise, 1-ground, 2-canopy, 3-top of canopy) were determined. [63]. The acquired photon data were subjected to a filtering process that selected photon data with medium and high signal confidence, as well as classification values of ground and top of canopy. All data of

between 2018 and 2022 belonging to tracks with IDs 777, 1196, and 1219 identified in the study area were examined. Data were identified that included urban areas and available building information. ICESat-2/ATLAS data that did not contain urban areas were not used for the study. The DSM generated from airborne LiDAR data and ICESat-2/ATLAS data was overlaid in ArcGIS v10.4 software. Buildings present in the ICESat-2/ ATLAS data have been detected, and the 96 buildings identified were designated as sample data. The overlaid ICESat-2/ATLAS and DSM are shown in Figure 3.6.

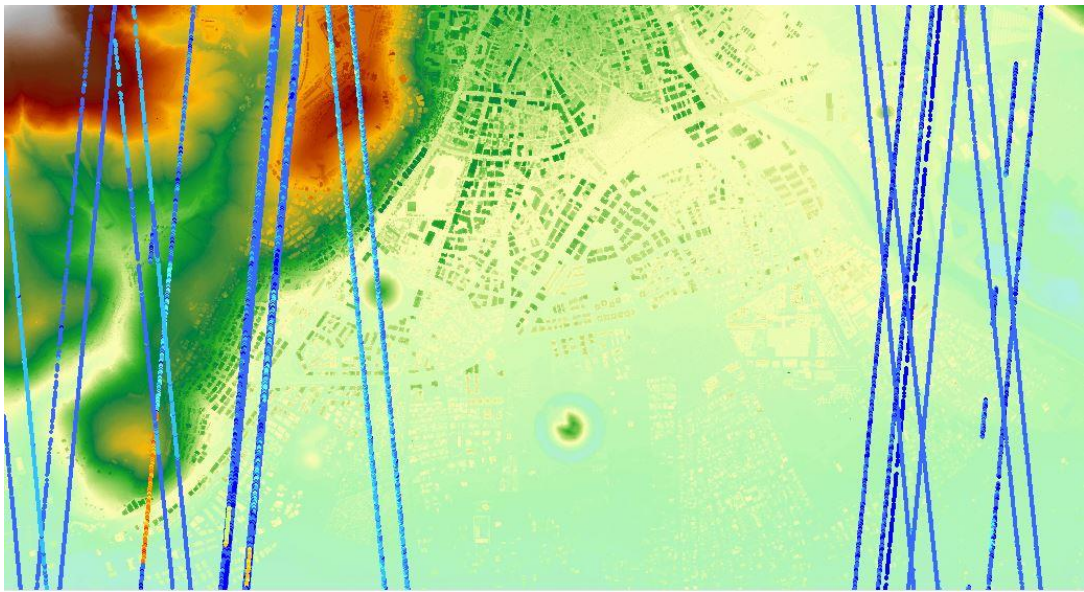


Figure 3.6: Overlaid ICESat-2/ATLAS and DSM.

Table 3.2: ICESat-2/ATLAS data and shift amounts on axes

ICESat-2/ATLAS Data	X-axis	Y-axis
ATL03_20191116183507_07770502_005_01_gt3l	-0.5 m	5.1 m
ATL03_20191116183507_07770502_005_01_gt3r	3.8 m	-2.4 m
ATL03_20200815053424_07770802_005_01_gt3l	1.7 m	-3.2 m
ATL03_20200815053424_07770802_005_01_gt3r	6.1 m	0.4 m
ATL03_20210212205409_07771002_005_01_gt1l	-1.1 m	-0.9 m
ATL03_20210212205409_07771002_005_01_gt1r	1.1 m	0.9 m
ATL03_20210212205409_07771002_005_01_gt2l	0.4 m	4.0 m
ATL03_20210212205409_07771002_005_01_gt2r	2.1 m	0.8 m
ATL03_20190316182741_11960206_005_01_gt2l	3.6 m	4.4 m

Table 3.2 (continued): ICESat-2/ATLAS data and shift amounts on axes

ATL03_20190316182741_11960206_005_01_gt2r	44.6 m	-3.9 m
ATL03_20190316182741_11960206_005_01_gt3l	0.9 m	1.1 m
ATL03_20190316182741_11960206_005_01_gt3r	2.8 m	2.3 m
ATL03_20190615140717_11960306_005_01_gt2l	0.9 m	1.1 m
ATL03_20190615140717_11960306_005_01_gt2r	2.7 m	3.3 m
ATL03_20200314010644_11960606_005_01_gt2l	0.0 m	0.0 m
ATL03_20200314010644_11960606_005_01_gt2r	0.2 m	-2.0 m
ATL03_20200612204628_11960706_005_01_gt2l	3.1 m	-0.7 m
ATL03_20200612204628_11960706_005_01_gt2r	1.1 m	-0.9 m
ATL03_20201211120608_11960906_005_01_gt2l	11.4 m	18.1 m
ATL03_20201211120608_11960906_005_01_gt2r	-18.5 m	36.4 m
ATL03_20201211120608_11960906_005_01_gt3l	2.4 m	6.3 m
ATL03_20201211120608_11960906_005_01_gt3r	-21.2 m	-52.2 m
ATL03_20210909230547_11961206_005_01_gt2l	2.0 m	0.2 m
ATL03_20210909230547_11961206_005_01_gt2r	0.2 m	-2.0 m
ATL03_20220310142533_11961406_005_01_gt2r	0.0 m	0.0 m
ATL03_20220908054524_11961606_005_01_gt3l	5.3 m	-35.7 m
ATL03_20220908054524_11961606_005_01_gt3r	0.9 m	1.1 m
ATL03_20190915213117_12190402_005_01_gt1l	1.5 m	-5.2 m
ATL03_20190915213117_12190402_005_01_gt1r	-1.7 m	3.2 m

3.2.3 Field Measurement Data

As part of the study, field measurements were made to determine the height of buildings consistent with ICESat-2/ATLAS data. GNSS measurements were made with the receiver “TOPCON GR-5” GPS, and building heights were measured with the total station “TOPCON OS-101” total station belonging to Izmir Katip Çelebi University. The technical specifications of the GNSS receiver and total station used in

the measurements are shown in Figure 3.7 and Figure 3.8, respectively. The heights of a total of 96 buildings were determined through field measurements, and the corresponding X and Y coordinates of these buildings were also recorded. The building heights obtained through field measurements are considered as reference data for the building heights obtained from ICESat-2 and airborne LiDAR data.

GNSS	
Signals Tracked	GPS: L1, L1C, L2, L2C, and L5 GLONASS: L1, L2 Galileo*: E1, E5a, E5b, AltBOC BeiDou: B1, B2 SBAS L1 C/A WAAS/MSAS/EGNOS QZSS L1 C/A, L1C, L2C
Number of Channels	226-Channel Vanguard Technology with Universal Tracking Channels capable of All-in-View tracking
Antenna Type	Integrated Fence Antenna (1) with Ground Plane
Accuracy	
Static	H: 3mm + 0.1ppm (2) V: 3.5mm + 0.4ppm (2)
RTK	H: 5mm + 0.5ppm V: 10mm + 0.8ppm



Figure 3.7: Specifications of the TOPCON GR-5.

Telescope	
Magnification / Resolving power	30x / 2.5"
Others	Length: 171mm (6.7in.), Objective aperture: 45mm (1.8in.) (48mm (1.9in.) for EDM), Image: Erect, Field of view: 1°30' (26m/1,000m), Minimum focus: 1.3m (4.3ft.), Reticle illumination: 5 brightness levels
Angle Measurement	
Display resolution	0.5" / 1" (0.0001 / 0.0002gon, 0.002 / 0.005mil)
Accuracy (ISO 17123-3:2001)	1"
Dual-axis compensator / Collimation compensation	Dual-axis liquid tilt sensor, working range: ±6' (±111mgon) / Collimation compensation available
Distance Measurement	
Laser output ^{*1}	Reflectorless mode: Class 3R / Prism / sheet mode: Class 1
Reflectorless ^{*2}	0.3 to 500m (1.0 to 1,640ft.)
Reflective sheet ^{*4/*5}	RS90N-K: 1.3 to 500m (4.3 to 1,640ft.) RSS0N-K: 1.3 to 300m (4.3 to 980ft.), RS10N-K: 1.3 to 100m (4.3 to 320ft.)
Accuracy	
Reflectorless ^{*3}	(3 + 2ppm x D) mm ^{*7}
Reflective sheet ^{*4}	(3 + 2ppm x D) mm
AP/CP prism	(2 + 2ppm x D) mm



Figure 3.8: Specifications of the TOPCON OS-101.

3.2.4 Classification Processing with Machine Learning Algorithms

Libraries have been added to the Spyder (Python v3.9) environment that are used to create data frames, properly access data, handle large datasets, and perform calculations using the 'import' command. The ICESat-2/ATLAS datasets with a (.csv) extension for which a classification task is desired has been loaded into the Spyder environment. The ICESat-2/ ATLAS data, filtered based on signal reliability and classification parameters, was split 70% for training and 30% for testing. The “KNeighborsClassifier” class from the “sklearn.neighbors” module was imported to perform classification using the K-NN machine learning algorithm. The necessary parameters for the classification were defined. The algorithm was trained on 70% of the training data. The remaining 30% of the data, reserved for testing, was used to make predictions. The process applied to the K-NN algorithm were also applied to the SVM, RF, ANN and RANSAC machine learning algorithms. For classification with the machine learning algorithm SVM, the class "SVC" is imported from the module "sklearn.svm". For classification with the Random Forest (RF) machine learning algorithm, the “RandomForestClassifier” class from the “sklearn.ensemble” module is imported. To perform classification using Artificial Neural Networks (ANNs), the “keras” module from “tensorflow”, the “Sequential” class from “tensorflow.keras.models”, and the “Dense” class from “tensorflow.keras.layers” are imported. Finally, for classification with the RANSAC algorithm, the “RANSACRegressor” class from the “sklearn.linear_model” module is imported. The parameters required for the classification are defined. The algorithm is trained on the training data and used for the predictions of the test data.

The airborne LiDAR data used in the study consists of a dense point cloud. To facilitate the classification process of these data using machine learning algorithms, it is necessary to clip the classified airborne LiDAR data. The clipping process was performed by overlaying the airborne LiDAR data with ICESat-2/ATLAS data. The airborne LiDAR data were clipped with reference to the ICESat-2/ATLAS data. CloudCompare v2.11 software was used for this process. The airborne LiDAR dataset1, which corresponds to the airborne LiDAR data coinciding with the ICESat-

2/ATLAS datasets has been loaded into the Spyder environment with the file extension (.csv). The airborne LiDAR data, filtered based on X, Y and Z coordinates and classification parameters, was split 67% for training and 33% for testing. The “KNeighborsClassifier” class from the “sklearn.neighbors” module was imported to perform classification using the K-NN machine learning algorithm. The necessary parameters for the classification were defined. The algorithm was trained on 67% of the training data. The remaining 33% of the data, reserved for testing, was used to make predictions. The parameters required for the classification are defined. The algorithm is trained on the training data and used for the predictions of the test data. The process applied to the K-NN algorithm were also applied to the SVM, RF, ANN and RANSAC machine learning algorithms.

3.2.5 Accuracy Analysis of Algorithms

The confusion matrix (Figure 3.9), also called error matrix, is used to evaluate the performance of algorithms in classification tasks. Actual values are compared to predicted values and various performance metrics are determined [65].

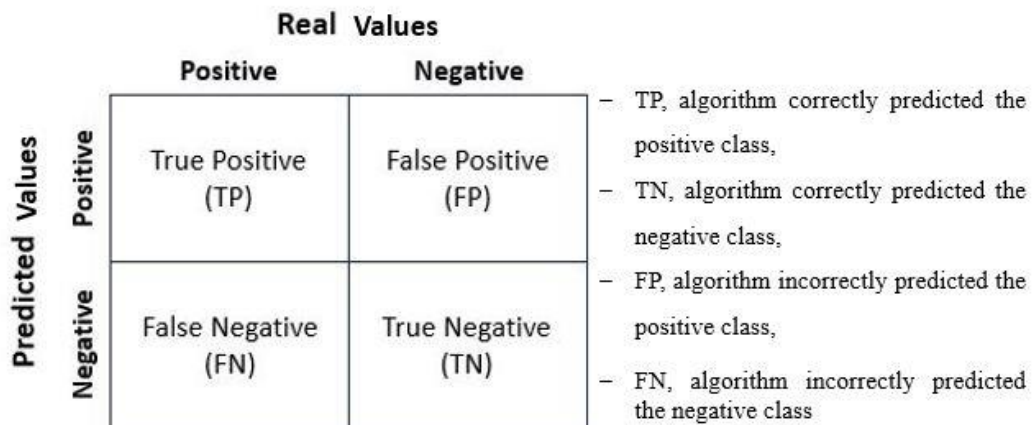


Figure 3.9: Confusion matrix.

Confusion matrices have been obtained for the K-NN, SVM, RF, ANN and RANSAC algorithms in the Spyder environment. These matrices are created using the test data set aside and the prediction results obtained from the classification process. The accuracies of the algorithms have been calculated using equation (3.1) based on the confusion matrix.

$$\text{Accuracy} = \frac{\sum TP + TN}{\sum TP + FP + FN + TN} \quad (3.1)$$

The accuracy rates of classification processes using K-NN, SVM, RF, ANN, and RANSAC algorithms for the ICESat-2/ATLAS and airborne LiDAR datasets were calculated using the confusion matrix shown in Figure 3.9.

Chapter 4

Results and Discussions

In this study, performance analyses of machine learning algorithms were conducted for calculating building heights using airborne LiDAR and ICESat-2 data. K-NN, SVM, RF, ANN and RANSAC machine learning algorithms were utilized for the classification of ICESat-2/ATLAS and airborne LiDAR data. The accuracy values calculated from the classification processes applied to ICESat-2/ATLAS data sets are given in Table 4.1. Similarly, accuracy values computed from the classification processes applied to airborne LiDAR data sets are presented in Table 4.2. (The airborne LiDAR data listed in Table 4.2 is presented in correspondence with the ranking of the ICESat-2/ATLAS data listed in Table 4.1).

Table 4.1: Accuracy analysis of the classification results of ICESat-2/ATLAS

ICESat-2/ATLAS Data	K-NN	SVM	RF	ANN	RANSAC
Strong Beams	0.9408	0.7543	0.9683	0.7760	0.7168
Weak Beams	0.9426	0.7211	0.9614	0.7546	0.6617

Table 4.2: Accuracy analysis of the classification results of airborne LiDAR

	K-NN	SVM	RF	ANN	RANSAC
Airborne LiDAR Dataset	0.9999	0.9111	0.9998	0.9848	0.5366

Within the scope of the study, a sample of 96 buildings was selected for the purpose of estimating building heights. For 16 of these buildings, sufficient data could not be obtained from the ICESat-2/ATLAS point cloud to determine their heights.

Additionally, the building heights could not be determined for 10 buildings that were identified as constructed after 2014, based on the acquisition date of the airborne LiDAR data. Consequently, based on these results, a total of 70 buildings had their heights determined using ICESat-2/ATLAS, airborne LiDAR, and field measurement data. The heights obtained for the 70 buildings are shown in Figure 4.1.

The linear regression model was used in the study to understand the relationship between building height data obtained from the systems used in the study and to analyze this relationship. Linear regression models were applied to the data obtained from pairs of field measurements - airborne LiDAR, field measurements - ICESat-2, and airborne LiDAR - ICESat-2. The model was developed to assess its performance by comparing the predictions made on test data with the actual test data.

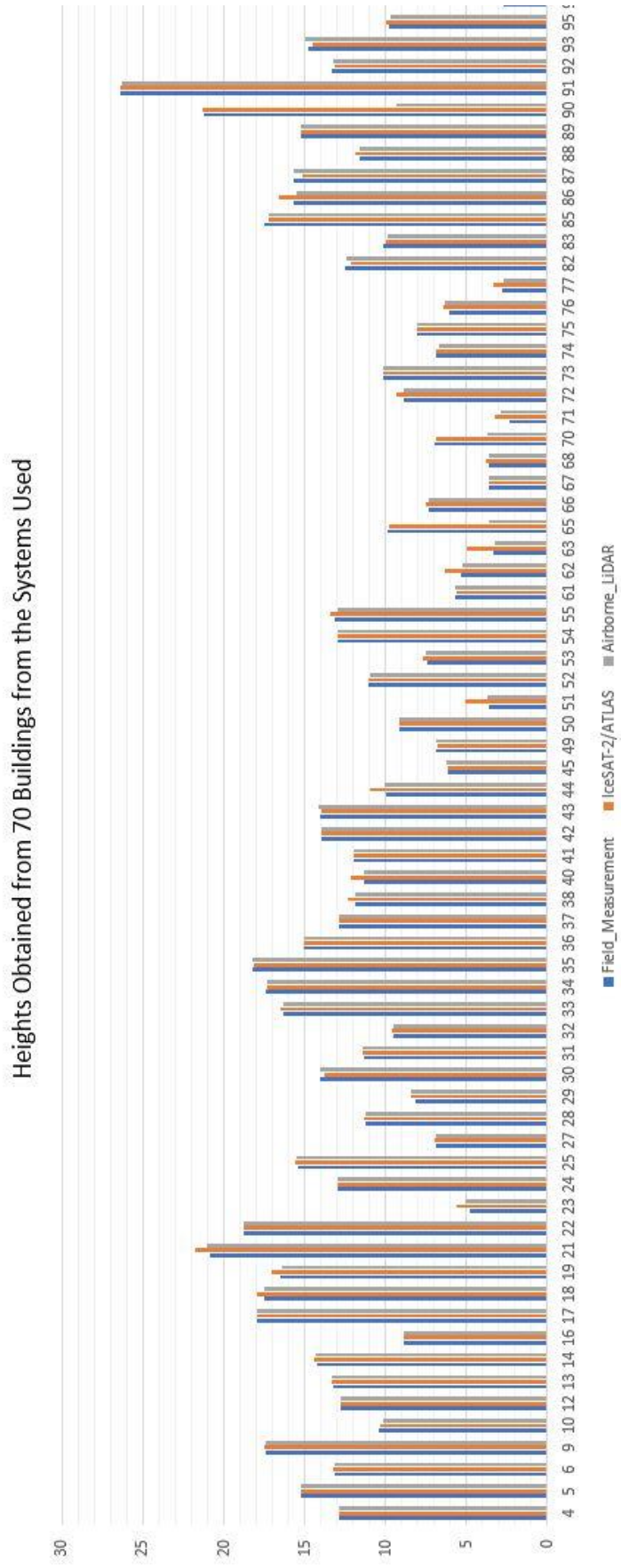


Figure 4.1: The heights obtained for the 70 buildings.

To measure the performance of the regression model, evaluate its reliability, and assess the accuracy of the predictions, the following metrics were calculated: R-squared (R^2) value, Root Mean Square Error (RMSE), Mean Squared Error (MSE), Mean Absolute Error (MAE), and Mean Error (ME). The regression model applied to field measurements - airborne LiDAR, field measurements - ICESat-2, and airborne LiDAR - ICESat-2 pairs, along with the calculated statistical values, are shown in Figure 4.2.

When examining the building heights obtained from the systems used, it was observed that the field measurements and ICESat-2 data were close for buildings numbered 65, 70, and 90. However, airborne LiDAR data tended to indicate lower heights for these buildings. Therefore, to explain this situation, photographs from the years 2016 and 2022 were examined. As a result of the investigations, it was determined that additional floors were added to buildings number 65 and 70. Additionally, it was found that a new building was constructed in place of building number 90. Photographs of building number 65 are provided in Figure 4.2, photographs of building number 70 are provided in Figure 4.3, and photographs of building number 90 are provided in Figure 4.4.



Figure 4.2: Photos of building number 65, (a) From 2016, (b) From 2022.



Figure 4.3: Photos of building number 70, (a) From 2016, (b) From 2022.

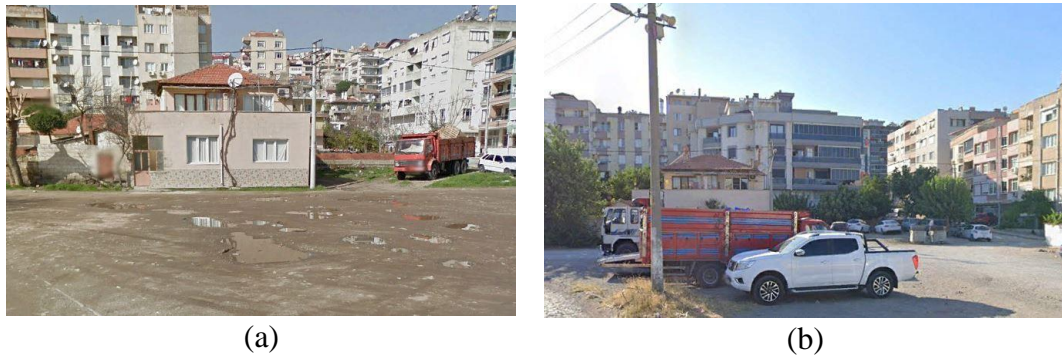


Figure 4.4: Photos of building number 90, (a) From 2016, (b) From 2022.

The reason for the differences in building heights obtained from airborne LiDAR data compared to the other two systems is that the airborne LiDAR data were collected in 2014 and do not reflect changes that occurred to these buildings after 2014. Therefore, the airborne LiDAR data does not represent the current heights of these structures, and this discrepancy was explained by the research conducted. As a result of these findings, the height data for buildings numbered 65, 70, and 90 were removed from the regression model, and a new regression model was created, which included height data for 67 buildings. To assess the performance of the newly created regression model, the following metrics were calculated: R^2 value, RMSE, MSE, MAE, and ME.

4.1 Field Measurement–Airborne LiDAR Accuracy Assessment

A linear regression model was built using height data for 70 different buildings based on field measurements and airborne LiDAR data. After identifying the outliers, a new regression model was created using height data for a total of 67 different buildings.

Error values for the created models were calculated. The regression models based on field measurements and airborne LiDAR data, along with their error values, are visually presented in Figure 4.5.

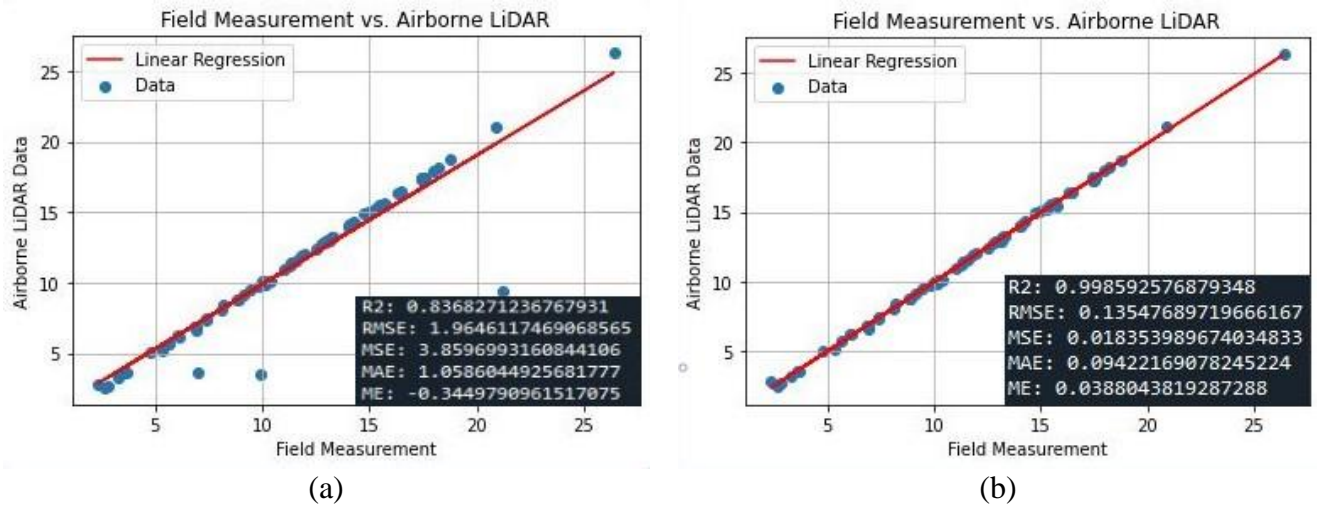


Figure 4.5: Field Measurement-Airborne LiDAR linear regression, (a) With height data of 70 buildings, (b) With height data of 67 buildings.

A regression model was developed based on field measurements and airborne LiDAR data, resulting in initial height predictions for 70 different buildings. The statistical values for these predictions were calculated as follows: $R^2 = 0.8368$, $RMSE = 1.9646$, $MSE = 3.8597$, $MAE = 1.0586$, and $ME = -0.3450$. After removing 3 identified outliers from the data set, a new regression model was created with height predictions for 67 different buildings. Statistical values for this updated model were calculated as follows: $R^2 = 0.9986$, $RMSE = 0.1355$, $MSE = 0.0184$, $MAE = 0.0942$, and $ME = 0.0388$.

These results suggest that the model obtained after removing outliers fits the data more closely and more reliably. A high R^2 coefficient means a strong alignment between the model and the observed data, indicating high predictive accuracy. The low values of $RMSE$, MSE , MAE , and ME indicate that the predictions of the model are closer to the actual data.

4.2 Field Measurement–ICESat-2/ATLAS Accuracy Assessment

A linear regression model was created between the height data of 70 buildings obtained from field measurement and ICESat-2/ATLAS data. After removing the identified outlier values, a new regression model was constructed using the height data of 67 buildings, and error values for the models were calculated. The regression models and error values for the field measurement and ICESat-2 data are shown in Figure 4.6.

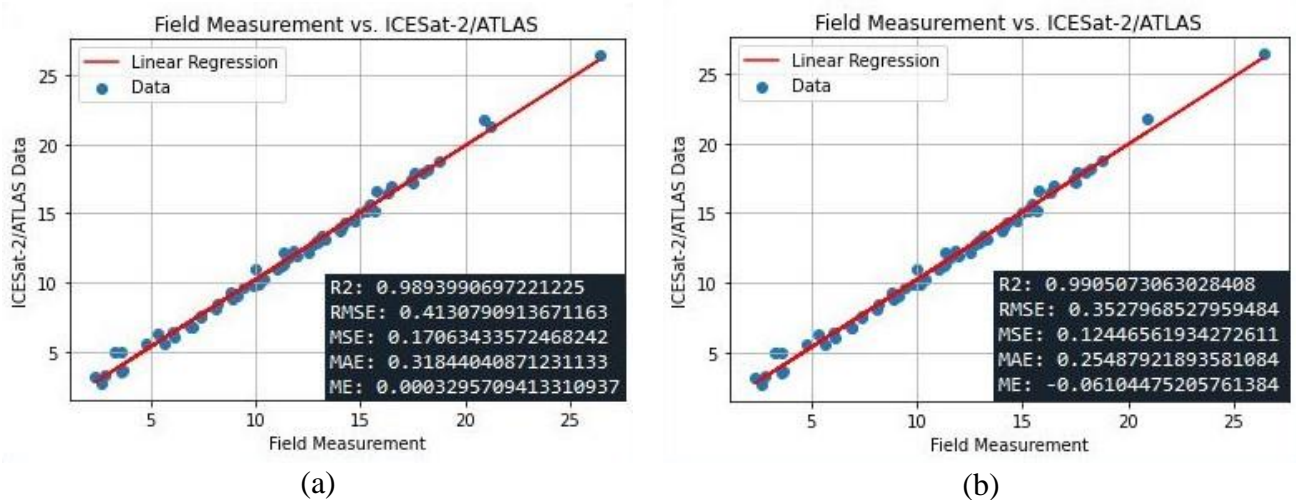


Figure 4.6: Field Measurement-ICESat-2/ATLAS linear regression, (a) With height data of 70 buildings, (b) With height data of 67 buildings.

The regression model based on the field measurement and ICESat-2 data resulted in height predictions for 70 different buildings. The statistical values of these predictions were calculated as $R^2 = 0.9894$, $RMSE = 0.4131$, $MSE = 0.1706$, $MAE = 0.3184$, and $ME = 0.0003$. After removing three outliers from the data set, the statistical values of the new regression model created using the height predictions of 67 different buildings were calculated as follows: $R^2 = 0.9905$, $RMSE = 0.3528$, $MSE = 0.1245$, $MAE = 0.2549$, and $ME = -0.0611$.

The results show that both the initial model and the new model created after removing the outliers are of high quality. An R^2 value of about 0.99 indicates that the model is in excellent agreement with the observed data. The low values of RMSE, MSE, MAE,

and ME indicate that the predictions of the model are very close to the actual data. The removal of outliers appears to have improved the accuracy of the model's predictions.

4.3 Airborne LiDAR–ICESat-2/ATLAS Accuracy Assessment

A linear regression model was constructed between the height data of 70 buildings obtained from aerial LiDAR and ICESat-2/ATLAS data. After removing the identified outlier values, a new regression model was created using the height data of 67 buildings and the error values for the models were calculated. The regression models and error values for aerial LiDAR and ICESat-2 data are shown in Figure 4.7.

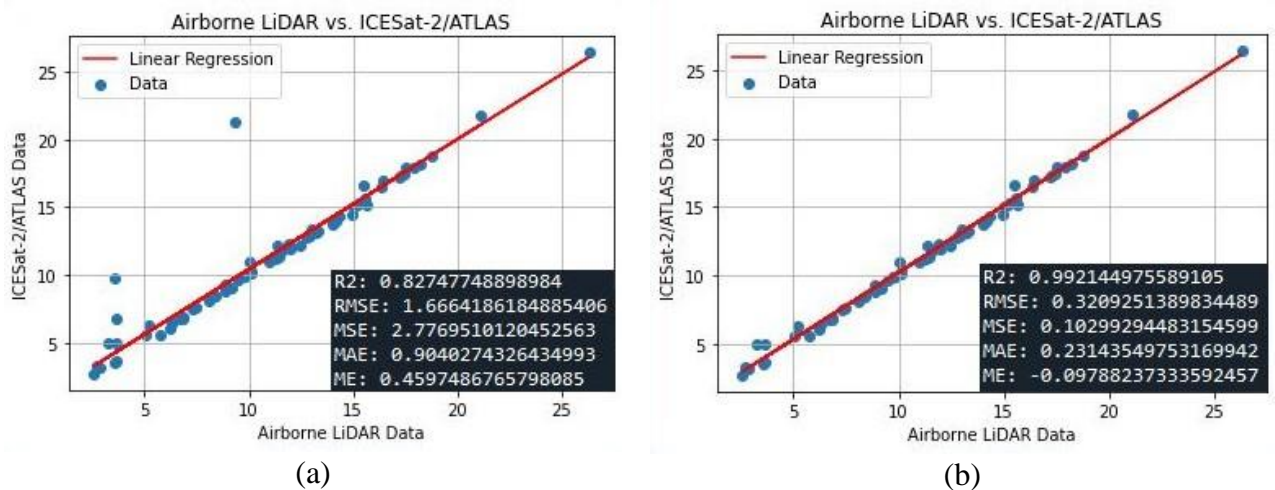


Figure 4.7: Airborne LiDAR-ICESat-2/ATLAS linear regression, (a) With height data of 70 buildings, (b) With height data of 67 buildings.

The regression model based on airborne LiDAR and ICESat-2 data produced height predictions for 70 different buildings. The statistical values of these predictions were calculated as $R^2= 0.8275$, $RMSE= 1.6664$, $MSE= 2.7770$, $MAE= 0.9040$, and $ME= 0.4598$. After removing three outliers from the data set, the statistical values of the new regression model created using the height predictions of 67 different buildings were calculated as follows: $R^2= 0.9922$, $RMSE= 0.3209$, $MSE= 0.1030$, $MAE= 0.2314$, and $ME= -0.0979$.

The results show that both the initial model and the new model created after removing the outliers are of high quality. An R^2 value of about 0.99 indicates that the model is in excellent agreement with the observed data. The low values of RMSE, MSE, MAE and ME show that the predictions of the model are very close to the actual data. The removal of outliers has improved the accuracy of the model's predictions.

Chapter 5

Conclusion

The objective of this study is to estimate building heights using machine learning algorithms based on airborne LiDAR and ICESat-2 data. The airborne LiDAR data were subjected to the necessary filtering processes to obtain digital models. ICESat-2 data were obtained from 2018 to 2022 within the study area. Digital models obtained from airborne LiDAR and ICESat-2 data were overlaid, and shifts in the ICESat-2/ATLAS data were determined. Airborne LiDAR and ICESat-2/ATLAS data were classified using K-NN, SVM, RF, ANN and RANSAC classification algorithms. The error values and accuracy rates of the classification methods were determined.

The analyses for ICESat-2 data performed show that the Random Forest classification algorithm has the highest accuracy rate. This result underlines the effective ability of the algorithm to classify data. The K-NN algorithm was found to have higher accuracy rates compared to the SVM, ANN and RANSAC algorithms for airborne LiDAR data. This result shows that the K-NN algorithm has better classification performance compared to other algorithms. In the literature, the RANSAC algorithm is commonly used for roof inference and object detection. It is assumed that this contributes to a lower accuracy in the classification processes. As a result of the classification processes performed on the Icesat-2 data, it was found that strong beams have higher accuracy rates compared to weak beams. This is thought to be due to the fact that strong beams have a denser point cloud. As the density of the point cloud increases, it can be deduced that the accuracy of the classification process improves. These analyses show that classification algorithms can deliver different results depending on the data type and features. Especially for special data types such as Icesat-2 data, data density should be considered as an important factor that can affect classification accuracy. In studies on the classification of ICESat-2/ATLAS data using machine

learning algorithms, researchers have found that the data obtained from the ICESat-2/ATLAS system in forested areas can be classified using K-NN, SVM, RF and GBDT machine learning algorithms. In the study conducted by Luo et al. [66] in a forested area, the RF algorithm was found to have the highest accuracy in classification.

When examining the study area and the data used, it is suspected that the presence of trees near buildings in urban areas could influence the classification results of the algorithms. This is due to the fact that the ICESat-2 dataset contains information on the photon class of top of canopy, which includes both tree and building data.

The building heights were determined using the data obtained from the systems. Regression models were created from the height data, including the following pairs: field measurement - airborne LiDAR, field measurement - ICESat-2/ATLAS and airborne LiDAR - ICESat-2/ATLAS. Statistical metrics were calculated on the basis of the regression models. For the 70 buildings, the regression models yielded the following R^2 values: 0.8368 for the field measurement-airborne LiDAR, 0.9894 for the field measurement-ICESat-2/ATLAS and 0.8275 for airborne LiDAR-ICESat-2/ATLAS. For the 67 buildings, the regression models yielded R^2 values of 0.9986 for field measurement-airborne LiDAR, 0.9905 for field measurement-ICESat-2/ATLAS and 0.9922 for airborne LiDAR-ICESat-2/ATLAS.

In the regression models created with the data from 70 buildings, the models that included airborne LiDAR data had lower R^2 values, but after removing outlier data from the models, an increase in R^2 values was observed. The airborne LiDAR data used in the study was collected during a flight in 2014 and therefore does not include recent changes to three buildings. This result underlines the importance of using up-to-date data in research.

The results obtained underline the reliability of LiDAR technologies and field measurements as a trustworthy data source for applications such as urban area characterization. This study shows how promising the ICESat-2 system is for future research in urban areas and offers a new perspective in the literature.

References

- [1] Ağca M. PALS, ICESat/GLAS ve ICESat-2 laser sistemleri ve kullanım alanları. *Geomatik Dergisi* 2020; 5(1): 27-35. doi.org/10.29128/geomatik.560344
- [2] Lohani B, Ghosh S. Airborne LiDAR technology: A review of data collection and processing systems. *Proceedings of the National Academy of Sciences, India Section A: Physical Sciences* 2017; 87: 567-579. doi.org/ 10.1007/s40010-017-0435-9
- [3] Neuenschwander AL, Urban TJ, Gutierrez R, Schutz BE. Characterization of ICESat/GLAS waveforms over terrestrial ecosystems: Implications for vegetation mapping. *Journal of Geophysical Research Atmospheres* 2008; 113. doi.org/10.1029/2007JG000557
- [4] Popescu S. Estimating biomass of individual pine trees using airborne lidar. *Biomass and Bioenergy* 2007; 31: 646–655. doi.org/10.1016/j.biombioe.2007.06.022
- [5] Schutz BE, Zwally HJ, Shuman CA, Hancock D, DiMarzio JP. Overview of the ICESat mission. *Geophysical Research Letters* 2005; 32 (21). doi.org/10.1029/2005GL024009
- [6] Wang X, Cheng X, Gong P, Huang H, Li Z, Li X. Earth science applications of ICESat/GLAS: a review. *International Journal of Remote Sensing* 2011; 32(23): 8837–8864. doi.org/10.1080/01431161.2010.547533
- [7] Zhang K, Chen S, Whitman D, Shyu M, Yan J, Zhang C. A progressive morphological filter for removing nonground measurements from airborne LIDAR data. *IEEE Transactions on Geoscience and Remote Sensing* 2003; 41(4): 872-882. doi.org/10.1109/TGRS.2003.810682

- [8] National Aeronautics and Space Administration. About GLAS [Online]. USA; [date of access 23.05.2023]. <https://attic.gsfc.nasa.gov/glas/about.html>.
- [9] Neuenschwander A, Guenther E, White JC, Duncanson L, Montesano P. Validation of ICESat-2 terrain and canopy heights in boreal forests. *Remote Sensing of Environment* 2020; 251, 112110. doi.org/10.1016/j.rse.2020.112110
- [10] National Aeronautics and Space Administration. About ICESat-2 [Online]. USA; 2019 [date of access 27.05.2023]. <https://www.nasa.gov/content/goddard/about-icesat-2>.
- [11] Wu Z. Estimating building height from ICESat-2 data: the case of the Netherlands (master's thesis). Netherlands: Delft University of Technology; 2022.
- [12] Markus T, Neumann T, Martino A, Abdalati W, Brunt K, Csatho B, *et al.* The Ice, Cloud, and land Elevation Satellite-2 (ICESat-2): Science requirements, concept, and implementation. *Remote Sensing of Environment* 2017; 190, 260-273. doi.org/10.1016/j.rse.2016.12.029
- [13] Nan Y, Feng Z, Liu E, Li B. Iterative Pointing Angle Calibration Method for the Spaceborne Photon-Counting Laser Altimeter Based on Small-Range Terrain Matching. *Remote Sensing* 2019; 11(18): 2158. doi.org/10.3390/rs11182158
- [14] National Snow and Ice Data Center. ICESat-2 Product Overviews [Online]. Colorado USA; 2023 [date of access 27.05.2023]. <https://nsidc.org/data/icesat-2/products>.
- [15] Hofmann-Wellenhof B, Lichtenegger H, Collins J. *Global Positioning System: Theory and Practice*, 4th ed. Wien, Austria: Springer-Verlag; 1997.
- [16] Montenbruck O, Gill E. (Ed.) *Satellite Orbits: Models, Methods and Applications*, 3rd ed. Springer; 2005.
- [17] Gopi S, Sathikumar R, Madhu N. *Advanced Surveying: Total Station, GPS, GIS and Remote Sensing*, 2nd ed. Pearson; 2018.

- [18] Alahmadi M, Atkinson P, Martin D. Estimating the spatial distribution of the population of Riyadh, Saudi Arabia using remotely sensed built land cover and height data. *Computers, Environment and Urban Systems* 2013; 41: 167-176. doi.org/10.1016/j.compenvurbsys.2013.06.002
- [19] Borck R. Will skyscrapers save the planet? Building height limits and urban greenhouse gas emissions. *Regional Science and Urban Economics* 2016; 58: 13-25. doi.org/10.1016/j.regsciurbeco.2016.01.004
- [20] Resch E, Bohne RA, Kvamsdal T, Lohne J. Impact of urban density and building height on energy use in cities. *Energy Procedia* 2016; 96: 800-814. doi.org/10.1016/j.egypro.2016.09.142
- [21] Yang X, Yuguo L. The impact of building density and building height heterogeneity on average urban albedo and street surface temperature. *Building and Environment* 2015; 90: 146-156. doi.org/10.1016/j.buildenv.2015.03.037
- [22] Tanikawa H, Fishman T, Okuoka K, Sugimoto K. The Weight of Society Over Time and Space: A Comprehensive Account of the Construction Material Stock of Japan, 1945–2010. *Journal of Industrial Ecology* 2015; 19(5): 778-791. doi.org/10.1111/jiec.12284
- [23] Perini K, Magliocco A. Effects of vegetation, urban density, building height, and atmospheric conditions on local temperatures and thermal comfort. *Urban Forestry & Urban Greening* 2014; 13(3): 495-506. doi.org/10.1016/j.ufug.2014.03.003
- [24] Polat N, Uysal M. Hava Lazer Tarama Sistemi, Uygulama Alanları ve Kullanılan Yazılımlara Genel Bir Bakış. *Afyon Kocatepe Üniversitesi Fen ve Mühendislik Bilimleri Dergisi* 2016; 16: 679-692. doi.org/10.5578/fmbd.41390
- [25] Antonarakis AS, Richards KS, Brasington J. Object-based land cover classification using airborne LiDAR. *Remote Sensing of Environment* 2008; 112(6): 2988-2998. doi.org/10.1016/j.rse.2008.02.004

- [26] Sefercik UG, Glennie C, Ateşoğlu A. Hava Kaynaklı Lazer Tarama Nokta Bulutları Kullanılarak 3B Meşcere Yükseklik Haritası Üretimi, Houston Örneği. TUFUAB VIII. Teknik Sempozyumu; 2015 Mayıs 21-23; Konya, Türkiye.
- [27] Guenther GC. Airborne Lidar Bathymetry. In: Maune, D. (Ed.), Digital Elevation Model Technologies and Applications: the DEM Users Manual, 2nd ed. American Society for Photogrammetry and Remote Sensing, Bethesda, Maryland; 2007. 253–320.
- [28] Magnoni A, Stanton TW, Barth N, Fernandez-Diaz JC, León JFO, Ruíz FP, *et al.* Detection Thresholds of Archaeological Features in Airborne Lidar Data from Central Yucatán. *Advances in Archaeological Practice* 2016; 4(3): 232-248. doi.org/10.7183/2326-3768.4.3.232
- [29] Bonczak B, Kontokosta CE. Large-scale parameterization of 3D building morphology in complex urban landscapes using aerial LiDAR and city administrative data. *Computers, Environment and Urban Systems* 2019; 73: 126-142. doi.org/10.1016/j.compenvurbsys.2018.09.004
- [30] González-Aguilera D, Crespo-Matellán E, Hernández-López D, Rodríguez-Gonzálvez P. Automated Urban Analysis Based on LiDAR-Derived Building Models. *IEEE Transactions on Geoscience and Remote Sensing* 2013; 51(3): 1844-1851. doi.org/10.1109/TGRS.2012.2205931
- [31] Zhou QY, Neumann U. Fast and extensible building modeling from airborne LiDAR data. In: Proceedings of the 16th ACM SIGSPATIAL international conference on Advances in geographic information systems; 2008 November; Irvine, California. 7-15. doi.org/10.1145/1463434.1463444
- [32] Wang X, Li P. Extraction of urban building damage using spectral, height and corner information from VHR satellite images and airborne LiDAR data. *ISPRS Journal of Photogrammetry and Remote Sensing* 2020; 159: 322-336. doi.org/10.1016/j.isprsjprs.2019.11.028

- [33] Zhang S, Han F, Bogus SM. Building Footprint and Height Information Extraction from Airborne LiDAR and Aerial Imagery. In: Construction Research Congress; 2020 March; Tempe, Arizona. 326-335.
- [34] Zhou Z, Gong J. Automated residential building detection from airborne LiDAR data with deep neural networks. *Advanced Engineering Informatics* 2018; 36: 229-241. doi.org/10.1016/j.aei.2018.04.002
- [35] Shirowzhan S, Sepasgozar SME, Li H, Trinder J, Tang P. Comparative analysis of machine learning and point-based algorithms for detecting 3D changes in buildings over time using bi-temporal lidar data. *Automation in Construction* 2019; 105: 102841. doi.org/10.1016/j.autcon.2019.102841
- [36] Neumann TA, Martino AJ, Markus T, Bae S, Bock MR, Brenner AC, *et al.* The Ice, Cloud, and Land Elevation Satellite – 2 mission: A global geolocated photon product derived from the Advanced Topographic Laser Altimeter System. *Remote Sensing of Environment* 2019; 233: 111325. doi.org/10.1016/j.rse.2019.111325
- [37] Petty AA, Kurtz NT, Kwok R, Markus T, Neumann TA. Winter Arctic Sea Ice Thickness From ICESat-2 Freeboards. *Journal of Geophysical Research: Oceans* 2020; 125(5). doi.org/10.1029/2019JC015764
- [38] Horvat C, Blanchard-Wrigglesworth E, Petty AA. Observing waves in sea ice with ICESat-2. *Geophysical Research Letters* 2020; 47(10). doi.org/10.1029/2020GL087629
- [39] Brunt KM, Neumann TA, Smith BE. Assessment of ICESat-2 Ice Sheet Surface Heights, Based on Comparisons Over the Interior of the Antarctic Ice Sheet. *Geophysical Research Letters* 2019; 46(2). doi.org/10.1029/2019GL084886
- [40] Ryan JC, Smith LC, Cooley SW, Pitcher LH, Pavelsky TM. Global characterization of inland water reservoirs using ICESat-2 altimetry and climate reanalysis. *Geophysical Research Letters* 2020; 47(17). doi.org/10.1029/2020GL088543

- [41] Wang C, Zhu X, Nie S, Xi X, Li D, Zheng W, *et al.* Ground elevation accuracy verification of ICESat-2 data: a case study in Alaska, USA. *Optics Express* 2019; 27(26):38168. doi.org/10.1364/OE.27.038168
- [42] Smith B, Fricker HA, Holschuh N, Gardner AS, Adusumilli S, Brunt KM, *et al.* Land ice height-retrieval algorithm for NASA's ICESat-2 photon-counting laser altimeter. *Remote Sensing of Environment* 2019; 233:111352. doi.org/10.1016/j.rse.2019.111352
- [43] Ma Y, Xu N, Liu Z, Yang B, Yang F, Wang XH, *et al.* Satellite-derived bathymetry using the ICESat-2 lidar and Sentinel-2 imagery datasets. *Remote Sensing of Environment* 2020; 250: 112047. doi.org/10.1016/j.rse.2020.112047
- [44] Aĝca M, Daloĝlu Aİ. Local Geoid height calculations with GNSS, airborne, and spaceborne Lidar data. *The Egyptian Journal of Remote Sensing and Space Science* 2023; 26(1): 85-93. doi.org/10.1016/j.ejrs.2022.12.009
- [45] Zhang Y, Pang Y, Cui D, Ma Y, Chen L. Accuracy Assessment of the ICESat-2/ATL06 Product in the Qilian Mountains Based on CORS and UAV Data. *IEEE Journal of Selected Topics in Applied Earth Observations and Remote Sensing* 2020; 14: 1558-1571. doi.org/10.1109/JSTARS.2020.3044463
- [46] Zhang J, Tian J, Li X, Wang L, Chen B, Gong H, *et al.* Leaf area index retrieval with ICESat-2 photon counting LiDAR. *International Journal of Applied Earth Observation and Geoinformation* 2021; 103:102488. doi.org/10.1016/j.jag.2021.102488
- [47] Tiwari K, Narine LL. A Comparison of Machine Learning and Geostatistical Approaches for Mapping Forest Canopy Height over the Southeastern US Using ICESat-2. *Remote Sensing* 2022; 14(22): 5651. doi.org/10.3390/rs14225651
- [48] Narine LL, Popescu SC, Malambo L. Synergy of ICESat-2 and Landsat for Mapping Forest Aboveground Biomass with Deep Learning. *Remote Sensing* 2019; 11(12): 1503. doi.org/10.3390/rs11121503
- [49] Lian W, Zhang G, Cui H, Chen Z, Wei S, Zhu C, *et al.* Extraction of high-accuracy control points using ICESat-2 ATL03 in urban areas. *International*

- Journal of Applied Earth Observation and Geoinformation 2022; 115: 103116.
doi.org/10.1016/j.jag.2022.103116
- [50] Dandabathula G, Sitiraju SR, Jha CS. Retrieval of building heights from ICESat-2 photon data and evaluation with field measurements. Environmental Research: Infrastructure and Sustainability 2021; 1(1). doi.org/10.1088/2634-4505/abf820
- [51] Zhao Y, Wu B, Shu S, Yang L, Wu J, Yu B. Evaluation of ICESat-2 ATL03/ATL08 Surface Heights in Urban Environments Using Airborne LiDAR Point Cloud Data. IEEE Geoscience and Remote Sensing Letter 2021; 19. doi.org/10.1109/LGRS.2021.3127540
- [52] Lao J, Wang C, Zhu X, Xi X, Nie S, Wang J, *et al.* Retrieving building height in urban areas using ICESat-2 photon-counting LiDAR data. International Journal of Applied Earth Observation and Geoinformation 2021; 104: 102596. doi.org/10.1016/j.jag.2021.102596
- [53] İnal C, Bülbül S, Yıldırım Ö. Ağ RTK ölçülerinin tekrarlanabilirliği. Afyon Kocatepe Üniversitesi Fen ve Mühendislik Bilimleri Dergisi 2014; 14: 1-7. doi.org/10.5578/fmbd.8548
- [54] El Naqa I, Murphy MJ. What is machine learning? Ed.: El Naqa I, Li R, Murphy MJ. Machine Learning in Radiation Oncology: Theory and Applications. Springer; 2015. 3-11.
- [55] National Aeronautics and Space Administration. ICESat-2/ Measuring the Height of Earth's Ice from Space [Pamphlet]. USA; 2016.
- [56] Cover T, Hart P. Nearest Neighbor Pattern Classification. IEEE Transactions on Information Theory 1967; 13(1): 21-27.
- [57] Mahesh B. Machine Learning Algorithms—A Review. International Journal of Science and Research 2020; 9(1): 381-386. doi.org/10.21275/ART20203995
- [58] Khan MMR, Arif RB, Siddique MAB, Oishe MR. Study and Observation of the Variation of Accuracies of KNN, SVM, LMNN, ENN Algorithms on Eleven Different Datasets from UCI Machine Learning Repository. ICEEICT:

Proceedings of the 2018 4th International Conference on Electrical Engineering and Information & Communication Technology; 2018 Sep 13-15; Dhaka, Bangladesh. 124–129.

- [59] Ren Q, Cheng H, Han H. Research on machine learning framework based on random forest algorithm. ACCS2015: Proceedings of the 11th Asian Conference on Chemical Sensors; 2015 Nov 16-18; Malaysia.
- [60] Zou J, Han Y, So SS. Overview of Artificial Neural Networks. Ed.: Livingstone DJ. Artificial Neural Networks: Methods and Applications. Humana Press; 2009. 14-22.
- [61] Imran M, Alsuhaibani SA. A Neuro-Fuzzy Inference Model for Diabetic Retinopathy Classification. Ed.: Hemanth DJ, Gupta D, Balas VE. Intelligent Data Analysis for Biomedical Applications: Challenges and Solutions. Academic Press; 2019. 147-172.
- [62] Fischler MA, Bolles RC. Random sample consensus: A paradigm for model fitting with applications to image analysis and automated cartography. Communications of the ACM 1981; 24(6): 381-395.
- [63] Neumann TA, Brenner A, Hancock D, Robbins J, Saba J, Harbeck K, *et al.* Algorithm Theoretical Basis Document (ATBD) for Global Geolocated Photons (ATL03), Version 3. National Snow and Ice Data Center Goddard Space Flight Center 2020; Greenbelt, Maryland.
- [64] Neuenschwander AL, Magruder LA. Canopy and Terrain Height Retrievals with ICESat-2: A First Look. Remote Sensing 2019; 11(14).
- [65] Visa S, Ramsay B, Ralescu A, Knaap E. Confusion Matrix-based Feature Selection. MAICS2011: Proceedings of The 22nd Midwest Artificial Intelligence and Cognitive Science Conference; 2011 April 16-17; Cincinnati, Ohio, USA.
- [66] Luo Y, Qi S, Liao K, Zhang S, Hu B, Tian Y. Mapping the Forest Height by Fusion of ICESat-2 and Multi-Source Remote Sensing Imagery and

Topographic Information: A Case Study in Jiangxi Province, China. *Forests*
2023; 14(3): 454. doi.org/10.3390/f14030454.

Appendix

Appendix

Publications from the Thesis

Conference Papers

1. Ağca M, Yücel A, Dalođlu A.İ., Kaya E, Yetkin M, Yalçın Küçükbayrak F. Estimation of Building Height from ICESat-2/ATLAS and Airborne LiDAR Data Using Machine Learning Algorithms. 2nd International Congress on Innovation Technologies & Engineering; 2023 June 12-13; Izmir, Turkey.

Projects

1. 1002–A Hızlı Destek Modülü, ICESat-2/Atlas ve Havasal Lidar Verilerinden Bina Yüksekliklerinin Hesaplanmasında Makine Öğrenmesi Algoritmalarının Performans Analizi (122Y415), Izmir Kâtip Çelebi University, 2023, Izmir, Turkey.

Curriculum Vitae

Name Surname : Aslıhan Yücel

Education:

2015–2020 İzmir Kâtip Çelebi University, Dept. of Geomatics Eng.

2020– İzmir Kâtip Çelebi University, Dept. of Geomatics Eng.

Work Experience:

2021 – Bornova Belediyesi (İzmir)